

國立臺灣大學醫學院暨工學院醫學工程學研究所

博士論文



Department of Biomedical Engineering  
College of Medicine and College of Engineering  
National Taiwan University  
Doctoral Dissertation

層粘連蛋白改質褐藻酸微米球包覆人參皂苷及脂肪衍生幹

細胞應用在乳房腫瘤切除術後乳房重建技術

Synthesis, Characterization, and Evaluation of Laminin-  
Alginate Microspheres Encapsulated with Ginsenoside Rg1  
and ADSCs for Breast Reconstruction after Lumpectomy

楊易軒

I-Hsuan Yang

指導教授：林峯輝 博士

陳右昇 博士

Advisor: Feng-Huei Lin, Ph.D.

Yo-Shen Chen, Ph.D.

中華民國 112 年 7 月

July 2023

國立臺灣大學博士學位論文  
口試委員會審定書

層粘連蛋白改質褐藻酸微米球包覆人參皂苷及脂肪衍生幹細胞應用在乳房腫瘤切除術後乳房重建技術

Synthesis, Characterization, and Evaluation of Laminin-Alginate Microspheres Encapsulated with Ginsenoside Rg1 and ADSCs for Breast Reconstruction After Lumpectomy

本論文係楊易軒君（學號 F07528014）在國立臺灣大學醫學工程學系完成之博士學位論文，於民國 111 年 04 月 25 日承下列考試委員審查通過及口試及格，特此證明

口試委員：

陳右昇	林孝輝
曾靖媛	(指導教授) 郭士元
陳克紹	黃義侑
	陳右昇

系主任：

吳東志



## 致謝

在碩士班接到博士班短短五年的時間裡，我要衷心感謝許多人的支持和協助，首先，我要先感謝我的父母和姐姐，感謝你們對我的無私和無盡的鼓勵，讓我其中一年在國外求學也能無後顧之憂的學習，讓我有機會追求學術的夢想。再來，我要感謝我的恩師林峯輝教授，您的細心指導和豐富的知識及經驗傳承，使我在研究項目上取得了豐碩的成果，感謝您對我的鼓勵和啟發，無論是研究上或是生活上的教導對我來說都是深刻且無價的。此外，我要感謝亞東醫院的陳右昇醫師和助理李佳靜，感謝你們對我研究中動物和臨床方面的支持和協助，你們的專業知識和寶貴的建議對我的研究結果和論文的完成起到了關鍵作用。其次，我要感謝日本 NIMS 荏原充宏教授，在我於日本 NIMS 度過的一年中，您是我在學術上的指導者，讓我可以打開我的國際觀，並且於各國的研究員充分交流、提供機會參與研討會、發表論文。同時，我也要感謝我求學過程中遇到的許多學長姊和學弟妹們，感謝台大的宇均學長、榮峰學長、煒堯學姊、雅鈞學姊、意文學姊、緻宇學長、子傑學長，還有國衛院的哲雍學長、志穎學長、奇翰學長、佳鼎學長等等，感謝你們總是不厭其煩的給予我人生和研究上的指導，從你們的身上我可以看到了許多成功的榜樣，著實給了我前進的動力。感謝跟我同屆的誼寧、一涵、侑玲、喻旋、欣然、逸恩，雖然你們比我早畢業，但是我們曾經一起的午餐、晚餐、爬玉山、去大陸找欣然等等事情都是我研究所中最美好的回憶。還有謝謝其他同輩的學生及學弟妹們，謝謝大家都在 Double 實驗室這個大家庭成長，彼此相互扶持，以至於讓實驗室如此的壯大。謝謝在日本 NIMS 遇到的每個台灣人和荏原實驗室的大家，讓我在異地求學時感受到第二個家般的溫暖，並且好好的成長了一番。


時光冉冉，轉眼間就到了我畢業的時間，希望我的尊師林峯輝老師和師母身體都能健康，事事順心，以及我的家人朋友們都能心想事成的完成自己的夢，我會牢牢記住您們對我的付出，並將此經驗好好傳承下去，謝謝大家，我們有緣的話下次再見！



## 摘要

乳房重建手術是讓女性罹患乳癌患者在進行手術切除乳房後的一種重建方式，儘管目前市面上已經有很多被開發的技術，但仍存在很多的問題，例如：義乳植入產生的異物反應造成莢膜攣縮、皮瓣手術所需的自體組織不足以及植入物易發生再吸收導致頻繁的手術需求等等。另一方面，組織工程已越來越被廣泛於研究中，利用組織工程來重建各個損傷部位已經成為了趨勢。本論文假說為使用幹細胞和可促進血管新生的小分子，同時包覆於生物材料之中形成微米球，與自體的脂肪細胞共混形成可注射的組織工程化脂肪組織，經過體內注射植入和數周的分化，幹細胞可以分化成脂肪細胞，促血管新生的小分子使組織間新生許多血管，可提高注射進去的細胞存活率以減緩植入物再吸收的情形。


本研究中，將透過低濃度的高碘酸鈉對褐藻酸進行改質，並將層粘連蛋白修飾於褐藻酸上，與培養基中的脂肪衍生幹細胞和人參皂苷 Rg1 共混，透過生物電噴灑技術，噴入氯化鈣溶液中，交聯形成層粘連蛋白改質褐藻酸微米球(ADSC-G-LAMS)。包覆脂肪衍生幹細胞和人參皂苷 Rg1 的微米球會與自體的脂肪細胞共混形成可注射的工程化脂肪組織，自體細胞釋放出的旁分泌訊號可以使脂肪衍生細胞走向脂肪新生分化。本實驗開發的材料備製成可注射的形式並用於乳房重建。利用傅立葉變換紅外分光光度計、光學顯微鏡、掃描式電子顯微鏡分別對 ADSC-G-LAMS 進行官能基鑑定、球尺寸量測和微結構的觀察；高效液相層析儀評估了人參皂苷 Rg1 從微米球中釋放情形；用 HUVEC 細胞體外管形成試驗評估從微米球釋放之人參皂苷 Rg1 的成血管能力；細胞活性、細胞毒性、基因毒性分別透過 WST-1，活/死染色和染色體結構異常分析進行評估，確認設計的 G-LAMS 的安全性；通過定量即時聚合酶鏈鎖反應確定 PI3K，Akt 和 eNOs 的基因表現量評估 G-LAMS 微米球的血管生成能力，將脂肪細胞和微米球結合以注射形式用於大鼠體內研究。用組織學染色和免疫螢光染色評估動物實驗結果；全血分析和血清學分析評估已開發的脂肪細胞和 ADSC-G-LAMS 微米球組合的安全性。



結果表明 ADSC-G-LAMS 微米球的大小約為 232.42  $\mu\text{m}$ ，提供一個很好的環境供細胞存活、生長，並不具任何的細胞毒性、基因毒性和全身性毒性。ADSC-G-LAMS 微米球擁有兩階段的藥物釋放，人參皂苷 Rg1 可以透過 PI3K/AKT/eNOs 路徑影響 HUVEC 細胞，並提升血管細胞 35.9% 的血管形成能力。動物實驗部分，本研究開發的 ADSC-G-LAMS 微米球可以很好地與宿主脂肪組織整合，持續釋放的人參皂苷 Rg1 造成組織具有適當血管生成能力，可應用於乳房重建手術。

關鍵字：層粘連蛋白改質褐藻酸微米球、脂肪衍生幹細胞、人參皂苷 Rg1、乳房重建手術、幹細胞療法。

## Abstract



Numerous advancements have been made in the field of breast reconstruction following lumpectomy. While these technologies have shown promising results in clinical settings, there are still several challenges that researchers must address. Tissue engineering has emerged as a potential solution for breast reconstruction after lumpectomy, offering hope to patients. In this study, a new approach utilizing laminin-modified alginate (abbreviated as ADSC-G-LAMS) was developed using a low concentration of sodium periodate. This modified alginate was mixed with ADSCs and Rg1 in a medium and then transformed into microspheres (ADSC-G-LAMS) using a bio-electrospray technique with a power syringe. The ADSC-G-LAMS microspheres were collected and combined with adipocytes to stimulate the production of necessary growth factors, guiding the ADSCs towards the adipogenic pathway. The resulting combination of ADSC-G-LAMS microspheres and adipocytes was prepared in an injectable form for breast reconstruction. The synthesized laminin-modified alginate microspheres loaded with Rg1 (G-LAMS) were characterized using various techniques such as Fourier transform infrared spectrophotometry (FTIR), optical microscopy, and scanning electron microscopy (SEM) to identify functional groups, measure sphere size, and examine microstructure, respectively. The release profile of Rg1 from the G-LAMS microspheres was evaluated using high-performance liquid chromatography (HPLC). The ability of the developed G-LAMS microspheres to support vascularization was assessed through the HUVEC tube formation assay using Matrigel<sup>TM</sup>. Safety evaluations, including cell viability, cytotoxicity, and genotoxicity, were conducted using WST-1, live/dead staining, and chromosome aberration tests, respectively. The angiogenic potential of the G-LAMS microspheres was assessed by analyzing gene expression levels of PI3K, Akt, and eNOS using real-time quantitative PCR (Q-PCR). An *in vivo* study using SD rats involved

combining the adipocytes and microspheres in an injectable form. The efficacy of the treatment was evaluated through hematoxylin & eosin (H&E) and immunofluorescence staining. Additionally, blood element analysis and serological analysis were conducted to assess the safety of the combined treatment of adipocytes and ADSC-G-LAMS microspheres. The results demonstrated that ADSC-G-LAMS microspheres successfully integrated with the host adipose tissue, promoting angiogenesis through the sustained release of Rg1 for breast reconstruction.

Key words: laminin-alginate microspheres, adipose-derived stem cells, ginsenoside Rg1, breast reconstruction, stem cell therapy.

# CONTENTS



致謝.....	i
摘要.....	ii
Abstract .....	iv
CONTENTS .....	vi
LIST OF FIGURES .....	ix
LIST OF TABLES .....	xiii
LIST OF ABBREVIATION.....	xiv
Chapter 1 INTRODUCTION .....	1
1.1 Incidence of breast cancer .....	1
1.2 Treatment of breast cancer.....	2
1.3 Breast reconstruction methods.....	2
1.3.1 Implants .....	2
1.3.2 Tissue flaps .....	3
1.3.3 Lipofilling.....	3
1.4 Soft tissue regeneration.....	3
1.5 Adipose tissue engineering .....	7
1.5.1 Cells.....	7
1.5.2 Scaffold.....	7
1.5.3 Signals .....	8
1.6 Purpose of the study .....	9
Chapter 2 THEORETICAL BASIS .....	11
2.1 Alginate.....	11
2.2 Laminin .....	12
2.3 Ginsenoside Rg1 .....	14



2.4	Cells .....	16
2.5	Bio-electrospray method .....	16
2.6	Materials design of the study.....	18
Chapter 3	MATERIALS AND METHODS .....	21
3.1	Experimental instruments .....	21
3.2	Experimental chemicals .....	22
3.3	Flow chart of the study .....	23
3.4	The synthesis of laminin-modified alginate.....	24
3.5	The preparation of laminin-modified alginate microsphere (LAMS) .....	24
3.6	The preparation of Rg1 encapsulated in LAMS microsphere (G-LAMS) .	25
3.7	The preparation of ADSC-G-LAMS microsphere.....	25
3.8	The analysis of Fourier transform infrared spectrophotometer (FTIR) .....	26
3.9	The analysis of nuclear magnetic resonance (NMR) .....	26
3.10	The size measurement and morphology observation of the developed ADSC-G-LAMS microspheres.....	26
3.11	The SEM examination of the ADSC-G-LAMS microspheres.....	27
3.12	Cytotoxicity of the G-LAMS microsphere .....	27
3.13	ADSCs viability in the ADSC-G-LAMS microspheres.....	27
3.14	Releasing profiles of Rg1 from G-LAMS .....	28
3.15	The tube formation ability of the released Rg1 .....	28
3.16	Effect of G-LAMS on HUVEC gene expression .....	29
3.17	To evaluate the genotoxicity of G-LAMS by chromosome aberration assay	30
3.18	<i>In vivo</i> study .....	31
3.19	Statistics .....	32
Chapter 4	RESULTS.....	33



4.1	FTIR functional groups analysis .....	33
4.2	<sup>1</sup> H NMR spectrophotometry analysis .....	34
4.3	The size measurement of the LAMS .....	35
4.4	The size measurement and SEM examination of the developed ADSC-G-LAMS microspheres .....	36
4.5	The cytotoxicity of G-LAMS .....	37
4.6	Releasing profiles of Rg1 from G-LAMS .....	39
4.7	The ability of the tube formation for the synthesized G-LAMS .....	40
4.8	Effect of G-LAMS on HUVEC gene expression .....	41
4.9	Evaluation of G-LAMS on genotoxicity chromosome aberration assay ...	43
4.10	Histological and Immunofluorescence Analysis .....	44
4.11	Blood element analysis and serological analysis .....	48
Chapter 5	DISCUSSION .....	51
Chapter 6	CONCLUSION .....	55
Chapter 7	REFERENCE .....	56
	Publication list .....	67



## LIST OF FIGURES



Fig.1.1 Trends in incidence rates for selected cancers by sex in the USA from 1975 to 2015 .....	1
Fig.1.2 The strategy of this study.....	10
Fig.2.1 Chemical structure of alginate and the mechanism of alginate gel formation in the presence of divalent cations. ....	11
Fig.2.2 Structure of laminin.....	13
Fig.2.3 Chemical reaction to synthesis of laminin-modified alginate. ....	14
Fig.2.4 Structure of the ginsenoside Rg1 .....	15
Fig.2.5 Rg1-mediated angiogenic mechanism in HUVEC. ....	16
Fig.2.6 Various modes of electrospray. ....	17
Fig.2.7 Taylor cone and related concepts.....	18
Fig.2.8 Bio-electrospray system in the study.....	18
Fig.2.9 Scheme illustration of ADSC-G-LAMS preparation and its applications on adipose tissue regeneration. ....	20
Fig.3.1 Flow chart of the study. ....	23
Fig.4.1 The FTIR spectrum of alginate and laminin-modified alginate. The absorption band at $1735\text{ cm}^{-1}$ confirmed that forming of aldehyde group (C=O). A new absorption band at $1470\text{ cm}^{-1}$ in laminin-modified alginate indicates the amide bond formation. Furthermore, the band at $2850\text{ cm}^{-1}$ and $2920\text{ cm}^{-1}$ corresponded to asymmetric and symmetric C-H vibrations were also strengthened after modification. ....	34
Fig.4.2 $^1\text{H}$ NMR spectrum of alginate and laminin-modified alginate. The peaks ranging from 3.66 to 4.99 ppm belonged to the protons of G and M units of the alginate peaks. Additional peaks appeared at 5.08 ppm and 5.13 ppm corresponded to a	

hemiacetalic proton formed from aldehyde and hydroxy group in the laminin-modified alginate.....	35
Fig.4.3 Construction of the device of the bio-electrospray system .....	36
Fig.4.4 Different sizes of the LAMS formed by different electrospray modes. (a) Microdripping mode, (b), (c) Cone-jet mode.....	36
Fig.4.5 Morphology and microstructure of laminin-alginate microspheres were observed by optical microscope and SEM. The image was taken by optical microscope at (a) Day 0, (b) Day 2, (c) Day 5, (d) Day 9 after ADSC-G-LAMS preparation. The arrows indicated the ADSCs encapsulated in G-LAMS. Scale bar = 200 $\mu$ m. SEM images were taken on Day 5 at (e) 600X magnification and (f) 2000X magnification.....	37
Fig.4.6 The cell viability of G-LAMS was evaluated by 3T3-L1 viability based on the guidance of ISO-10993; the results would be in terms of cytotoxicity. ....	38
Fig.4.7 ADSCs in ADSC-G-LAMS were evaluated by live/dead staining assay. ADSCs were encapsulated in G-LAMS and analyzed at (a) Day 1, and (b) Day 5. The living cells color in green were stained with calcein AM and dead cells color in red were stained with ethidium homodimer-1. Scale bar = 100 $\mu$ m.....	39
Fig.4.8 Releasing profiles of Rg1 from G-LAMS. The cumulative Rg1 released curve was evaluated by HPLC analysis over time.....	40
Fig.4.9 The ability of the tube formation of the released Rg1 was tested by HUVEC tube formation assay with Matrigel <sup>TM</sup> (a) Control: medium with 2% FBS (b) Positive control: medium with 2% FBS and endothelial cell growth supplement (ECGS) (c) G-LAMS: medium with 2% FBS and released Rg1 from G-LAMS without ECGS. (d) Quantification by ImageJ software. ( $p < 0.05$ , *; $p < 0.001$ , ***, compared to control group by one-way ANOVA with Tukey's multiple	

comparisons test.).....	41
Fig.4.10 Gene expression of HUVECs after starvation for 4 hours and then treated with materials for 1 hour. Relative (a) PIK3CA (b) PIK3R1 (c) AKT3 (d) eNOs gene expression was measured by Q-PCR and normalized by GAPDH gene expression. ( $p < 0.05$ , *; $p < 0.01$ , **; $p < 0.001$ , *** compared to control group; $p < 0.05$ , #; $p < 0.01$ , ##; $p < 0.001$ , ### compared to LAMS group by one-way ANOVA with Tukey's multiple comparisons test.).....	42
Fig.4.11 The evaluation of the genotoxicity assay was determined by CHO cells chromosome aberration assay. CHO cells were treated by (a) negative control observed under 40X magnification and (b) negative control examined under 100X magnification; the aberrations would be compared with (c) experimental group added with G-LAMS extract observed under 40X magnification and (d) experimental group added with G-LAMS extract observed under 100X magnification.....	43
Fig.4.12 Oil Red O staining image of the adipogenic differentiation induced ADSCs. Scale bar = 20 $\mu$ m.....	45
Fig.4.13 <i>In vivo</i> analysis of grafts after 4 weeks (a) Immunofluorescence staining of CD31 on adipose tissue sections from the implant site. CD31 was used as an endothelial cell marker. Nuclei were stained with DAPI, and GFP-positive cells were observed by confocal microscopy. In H&E staining, arrows indicate blood vessels, and asterisks indicate the implanted microspheres. Scale bar = 100 $\mu$ m, (b) Quantification of angiogenesis was determined by calculating relative cell number in CD31 fluorescence image by ImageJ. (Data in (b) were measured by four independent experiments, and at least five fields were taken per section.) ( $p < 0.05$ , *; $p < 0.01$ , **; $p < 0.001$ , ***, compared to the ADSC–adipocyte group; $p < 0.05$ ,	

#;  $p < 0.01$ , ##;  $p < 0.001$ , ### compared to the ADSC–LAMS–adipocyte group by one-way ANOVA with Tukey's multiple comparisons test.)..... 46

Fig.4.14 The pictures of implanted materials after 4 weeks of transplantation. (a) Represented picture of the rats (ADSC–G–LAMS–adipocyte group) *in vivo* study. The black arrow indicated the implanted materials. (b) ADSC–adipocyte group. (c) ADSC–LAMS–adipocyte group. (d) ADSC–G–LAMS–adipocyte group. Scale bar = 1 cm. .... 47

Fig.4.15 The graft volume of implanted materials after 4 weeks of transplantation. ( $p < 0.05$ , \*,  $p < 0.01$ , \*\*, compared to the ADSC–adipocyte group;  $p < 0.05$ , #, compared to ADSC–LAMS–adipocyte group.) ..... 48

## LIST OF TABLES



Table 1.1 FDA-approved dermal fillers. ....	5
Table 3.1 Experimental instrument, manufacturers, and model.....	21
Table 3.2 Experimental chemicals .....	22
Table 3.3 Primers for Real-time PCR .....	29
Table 4.1 The chromosome aberration data of the negative control group and the G-LAMS treated CHO cells. ....	44
Table 4.2 Summary of blood element analysis.....	49
Table 4.3 Summary of serological analysis. ....	50

## LIST OF ABBREVIATIONS

ADSC	Adipose-derived stem cells
ADSC-G-LAMS	ADSC+Rg1+Laminin-alginate microspheres
ADSC-G-LAMS-adipocyte	Mix ADSC+Rg1+Laminin-alginate microspheres with autologous adipocytes
AKT3	Serine/threonine-protein kinase
CHO	Chinese hamster ovary cell
CPD	Critical point dryer
eNOs	Endothelial nitric oxide synthase
FTIR	Fourier transform infrared spectrophotometer
G-LAMS	Rg1+Laminin-alginate microspheres
HPLC	High-performance liquid chromatography
HUVECs	Human umbilical vein endothelial cell
LAMS	Laminin-alginate microspheres
NMR	Nuclear magnetic resonance
PIK3CA	Phosphatidylinositol 3'-kinase (PI3K) catalytic subunit p110 $\alpha$
PIK3R1	PI3K regulatory subunit p85 $\alpha$
SEM	Scanning electron microscope
WST-1	Water soluble tetrazolium-1
Q-PCR	Quantitative polymerase chain reaction



# Chapter 1 INTRODUCTION



## 1.1 Incidence of breast cancer

Cancer is one of the causes of death worldwide. Fig.1.1 illustrates the trends in incidence rates for selected cancers by gender in the USA from 1975 to 2015 [1]. Among females, the most common cancer is breast cancer. In 2019, breast cancer accounts for 30% of all new cancer diagnoses in the United States [1]. The probability of a woman in the United States suffering from breast cancer during their lifetime is about 13%, which means that one in eight women will suffer from breast cancer sometime in her life [2]. Even in Taiwan, the incidence of breast cancer is still rising. 1 in 120 women in Taiwan has breast cancer [3]. Although the mortality rate of breast cancer is stable, it is also very important to choose a suitable treatment.

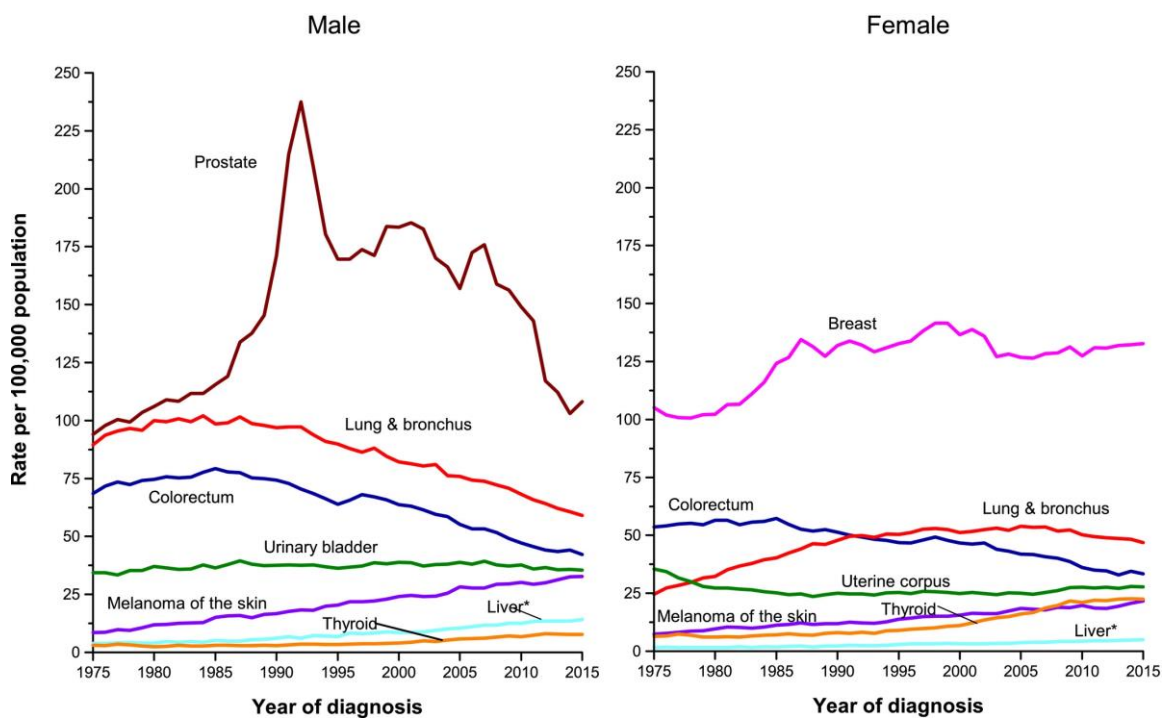
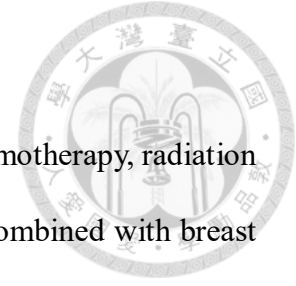


**Fig.1.1** Trends in incidence rates for selected cancers by sex in the USA from 1975 to 2015 [1].



## **1.2 Treatment of breast cancer**

In clinical, patients suffering from breast cancer can choose chemotherapy, radiation therapy, and hormone therapy. In most cases, they still need to be combined with breast cancer surgery, such as mastectomy or lumpectomy [4]. Lumpectomy, which can be also called breast-conserving surgery. The goal is to retain as much healthy breast tissue as possible. In this case, cancer did not develop to the whole breast, and only part of the tissue needs to be removed. In contrast, mastectomy has to remove the total breast from the patients when cancer has expanded rapidly. Since women often worry about aesthetics, the demand for breast reconstruction is one of the critical issues after surgery. In clinical, several methods have been developed for breast reconstruction.

## **1.3 Breast reconstruction methods**

### **1.3.1 Implants**

The silicone-based implants are the earliest and most common methods for breast reconstruction, such as saline implants and silicone implants filled with silicone gel. In 1961, Dr. Cronin and Gerow developed the first silicone breast implant [5]. They created the different viscosities of the materials to mimic different situations. In 1964, Laboratoires Arion, a French company, manufactured and launched the first saline-filled implants to enlarge the breast size [6]. After entering the US market in 1964, surgeons began to widely use breast implants, and breast augmentation surgery soon became one of the most popular cosmetic surgery in the United States. However, the implants are foreign bodies; that might induce serious foreign body reactions such as thick fibrous encapsulation to generate stress between implants and surrounding tissue. The stress may cause capsular contraction, implant rupture & leakage, poor tactile quality, and even unnatural shape [4, 7, 8].



### 1.3.2 Tissue flaps

In the late 1970s, tissue flap and free flap were to use as autologous tissue for breast reconstruction. These tissue flaps could be harvested from the abdomen, upper backs, thighs, and buttocks [9]. Compared to breast implants, tissue flaps generally look more natural and behave more likely to the natural tissue. Besides, there is no risk of implant rupture. However, the limitation of the flaps is that there are not so many donor sites for this procedure and the complications are about 30% after transplantation [4, 10, 11].

### 1.3.3 Lipofilling

Lipofilling technology is to collect a patient's fat as a fat graft by liposuction and then transplants into a lumpectomy site as autologous implants. Nevertheless, lipofilling is not very popular due to the unpredictable resorption rate and calcified tissue generation about 4-6 months post-surgery. In addition, the delayed or few neo-vascularization causes the inner part of the fat to undergo cell necrosis, fibrosis, and eventually volume loss; those scenarios limit the technology to be applied in breast reconstruction [12].

## 1.4 Soft tissue regeneration

Similar to breast reconstruction, nowadays FDA had approved some medical products for cosmetic surgery. Soft tissue fillers (or often called dermal fillers) are introduced in this method. Fillers can be permanent or temporary in the body and are classified into three categories: natural polymers and synthetic polymers. Table 1.1 list all FDA-approved dermal fillers. Most soft tissue fillers temporarily stay in the body, then followed by absorbed by the body over time. Only one filler made from the non-degradable materials, polymethylmethacrylate had been approved by FDA. Some soft tissue fillers also contain lidocaine to relieve the pain during the injection of the materials.

Although there are not any soft tissue fillers are used in breast augmentation after breast surgery, due to the failure of regulators of implantable medical devices to conform with FDA standards [13]. It still gives us the concept of using biomaterials could be a potential way for breast reconstruction.

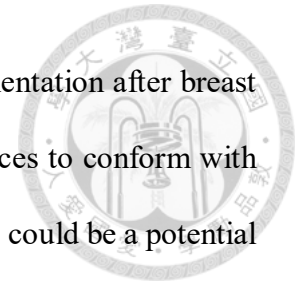
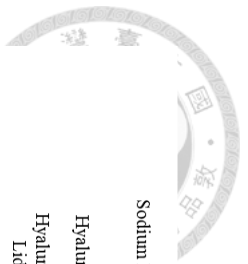




**Table 1.1 FDA-approved dermal fillers [14].**

Fillers type	Materials	Trade name	Applicant	Approval date	Indication for
Natural polymers	Hyaluronic Acid	RESTYLANE INJECTABLE GEL	Q-med Ab	12/12/2003	Mild to deep dermis for correction of moderate to severe facial wrinkles and folds.
	Modified hyaluronic acid derived from a bird (avian) source	HYLAFORM (HYLAN B GEL)	Genzyme Biosurgery	4/22/2004	Mild to deep dermis for correction of moderate to severe facial wrinkles and folds.
	Hyaluronic Acid	CAPTIQUE INJECTABLE GEL	Genzyme Biosurgery	11/12/2004	Mild to deep dermis for correction of moderate to severe facial wrinkles and folds.
	Hyaluronic Acid	RESTYLANE INJECTABLE GEL External Link Disclaimer	Medicus Aesthetics Holdings, Inc	3/25/2005	Mild to deep dermis for correction of moderate to severe facial wrinkles and folds.
	Hyaluronic Acid		JUVEDERM 24HV, JUVEDERM 30, and JUVEDERM 30HV	6/2/2006	Mild to deep dermis for correction of moderate to severe facial wrinkles and folds.
	Hyaluronic Acid with Lidocaine	Anika Therapeutics	ELEVESS	12/20/2006	Mild to deep dermis for correction of moderate to severe facial wrinkles and folds.
	Hyaluronic Acid with Lidocaine	Genzyme Biosurgery	PREVELLE SILK	2/26/2008	Mild to deep dermis for correction of moderate to severe facial wrinkles and folds (such as nasolabial folds).
	Hyaluronic Acid with Lidocaine	Allergan	JUVEDERM ULTRA XC, JUVEDERM ULTRA PLUS XC	1/7/2010	The addition of 0.3% Lidocaine into Juvederm Ultra and Juvederm Ultra Plus.
	Hyaluronic Acid	Medicus Aesthetics Holdings, Inc	RESTYLANE INJECTABLE GEL	10/11/2011	Lip augmentation in those over the age of 21 years.
	Hyaluronic Acid	Merz Pharmaceuticals	BELOTERO BALANCE	11/14/2011	Facial tissue to smooth wrinkles and folds, especially around the nose and mouth.
	Hyaluronic Acid with Lidocaine	Medicus Aesthetics Holdings, Inc.	RESTYLANE-L INJECTABLE GEL	8/30/2012	Mild to deep dermis for correction of moderate to severe facial wrinkles/folds and for lip augmentation in those over the age of 21 years.
	Hyaluronic Acid with Lidocaine	Allergan	JUVEDERM VOLUMA XC	10/22/2013	Deep (subcutaneous and/or supraperiosteal) injection for cheek augmentation to correct age-related volume deficit in the mid-face in adults over the age of 21.
	Hyaluronic Acid with Lidocaine	Valiant Pharmaceuticals North America LLC/Medicis	RESTYLANE SILK	6/13/2014	Lip augmentation and dermal implantation for correction of perioral rhytids in patients over the age of 21.
	Hyaluronic acid with Lidocaine	Galderna Laboratories	RESTYLANE LYFT WITH LIDOCAINE	7/1/2015	Severe facial folds and wrinkles or in patients over the age of 21 who have age-related volume loss.
	Hyaluronic Acid with Lidocaine	Allergan	JUVEDERM VOLBELLA XC	5/31/2016	Lip augmentation and for correction of perioral rhytids in adults over the age of 21.



Sodium Hyaluronate	Q-Med AB	Restylane, Refyne, Restylane Defyne	12/9/2016	Restylane Refyne is indicated mid-to-deep dermis for the correction of moderate to severe facial wrinkles and folds in patients over the age of 21. Restylane Defyne is indicated for mid-to-deep dermis for the correction of moderate to severe deep facial wrinkles and folds in patients over the age of 21.
Hyaluronic Acid	Allergan	JUVEDERM VOLUME XC	3/17/2017	Mild to deep dermis for correction of moderate to severe facial wrinkles and folds in adults over the age of 21.
Hyaluronic Acid, Lidocaine	Teoxane S.A.	RHA 2, RHA 3, RH 4	10/19/2017	Mid-to-deep dermis for the correction of moderate to severe dynamic facial wrinkles and folds, such as nasolabial folds, in adults aged 22 years or older
Hyaluronic Acid, Lidocaine	Prolunium Medical Technologies Inc.	Revanesse Versa +	8/2/2018	Mild to deep dermis for correction of moderate to severe facial wrinkles and folds, such as nasolabial folds, in adults 22 years of age or more
Hyaluronic Acid, Lidocaine	Prolunium Medical Technologies Inc.	Revanesse Versa	8/4/2018	Mild to deep dermis for correction of moderate to severe facial wrinkles and folds, such as nasolabial folds, in adults 22 years of age or more
Hyaluronic Acid, Lidocaine	Q-Med AB	Restylane Lyft with Lidocaine	5/18/2018	Deep dermis to superficial subcutis for the correction of moderate to severe facial folds and wrinkles, and correction of age-related midface contour deficiencies in patients over the age of 21, and for injection into the subcutaneous plane in the dorsal hand to correct volume deficit in patients over the age of 21.
Collagen	Allergan	ZYDERM COLLAGEN IMPLANT	9/18/1981	Dermis for correction of contour deficiencies of this soft tissue.
Collagen	Collagen Corp.	ZYPLAST(R)	6/24/1985	Mild to deep dermal tissues for correction of contour deficiencies.
Collagen	Serono Laboratories	FIBREL	2/26/1988	The correction of depressed cutaneous scars which are distensible by manual stretching of the scar borders.
Collagen	Inamed Corporation	COSMODERM 1 HUMAN-BASED C	3/11/2003	Superficial papillary dermis for correction of soft tissue contour deficiencies, such as wrinkles and acne scars.
Collagen	Colbar Lifescience 1	EVOLENCE COLLAGEN FILLER	6/27/2008	The correction of moderate to deep facial wrinkles and folds.
Synthetic polymers	Poly-L-Lactic Acid (PLLA)	Sanofi Aventis U.S.	8/3/2004	Restoration and/or correction of the signs of facial fat loss (facial lipoatrophy) in people with Human Immunodeficiency Virus (HIV).
Poly-L-Lactic Acid (PLLA)	Sanofi Aventis U.S.	SCULPTRA	7/28/2009	Use in shallow to deep nasolabial fold contour deficiencies and other facial wrinkles.
Hydroxylapatite	Bioform Medical, Inc	RADESSE 1.3CC AND 0.3CC	12/22/2006	Restoration and/or correction of the signs of facial fat loss (lipoatrophy) in people with HIV. Subdermal implantation for correction of moderate to severe facial wrinkles and folds.
Hydroxylapatite	Bioform Medical, Inc.	RADESSE	6/4/2015	Subdermal implantation for hand augmentation to correct volume loss in the dorsum of the hands.
Polymethylmethacrylate Beads, Collagen and Lidocaine.	Sumera Medical, Inc.	ARTEFILL	10/27/2006	Use in facial tissue around the mouth.



## 1.5 Adipose tissue engineering

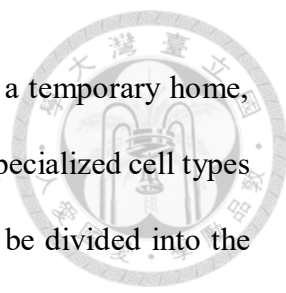
From the previous description, many technologies were developed for breast reconstruction after mastectomy or lumpectomy. Although the technologies achieved promising success in clinical, there are still many shortages hanging over and trouble the researchers. In 1998, tissue engineering technology was introduced to plastic surgery that gave light to mastectomy patients to overcome the previous shortages by adipose tissue engineering for breast reconstruction [15].

### 1.5.1 Cells

Some preadipocytes cell lines, like 3T3-L1 and Ob17 cell lines, could differentiate to adipocytes under specific inductions [16, 17]. These cell lines could harvest and proliferate rapidly in the laboratory culturing methods. These types of cells may be a good method for preliminary testing of the efficacy of other materials, but that could be impossible that use these cell lines for humans' breast reconstruction methods.

On the other hand, mesenchymal stem cells isolated from the patients' bodies in autologous form have been widely studied. Human bone marrow-derived mesenchymal stem cells (hBMSCs) and human adipose-derived mesenchymal stem cells (hADSCs) are two common cell sources in adipose tissue engineering [18]. Both kinds of cells are multipotent cells and can undergo self-renew and differentiate into specialized cell types [4, 19]. One disadvantage of using the hBMSCs is that the patients may be very painful when obtaining the bone marrow extraction. In contrast, hADSCs could be isolated easily by collecting the patients' fat and centrifuge processes. Therefore, in the past few years, hADSCs have become the main cell source for adipose tissue engineering. [18].

### 1.5.2 Scaffold

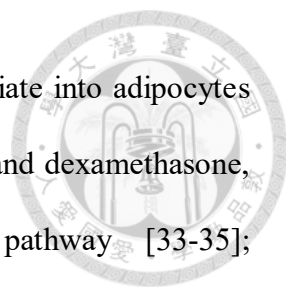


From the perspective of tissue engineering, the scaffold acts as a temporary home, providing cells with attachment, proliferation, and differentiation to specialized cell types within the scaffold [4]. By different applications form scaffolds can be divided into the bulk scaffold and injectable materials. Bulk scaffolds were usually made from porous 3D materials. Their advantage relies on they could have good geometric control via predefined shapes. However, because it is still bulk material, it still needs surgery for implantation, which may leave scars. The other is in situ injectable materials, which include injectable microspheres or hydrogel. The main advantage is that it can adapt to complex voids. At the same time, it can be implanted by injection and belongs to a minimum invasive approach [20].

The scaffolds could also be divided into synthetic polymers and natural polymers upon different sources of materials. For the synthetic polymers, biodegradable polyesters, such as polyglycolide, polylactide, and their copolymers were the most commonly used in adipose tissue regeneration [21-25]. Other biodegradable materials, including polycaprolactones, polyanhydrides, poly(amino acid)s, and poly(ortho ester)s were also studied and fabricated for adipose tissue reconstruction [26]. However, these polymers lack areas for cell identification, limiting cell growth and attachment of cells [27, 28]. To overcome these shortages, naturally derived polymers such as collagen [29], hyaluronic acid [30], gelatin [31], alginate [32] have been studied for adipose tissue regeneration. Natural polymers are usually found as part of the native ECM or their derived materials. The benefit of using natural materials relies on good biocompatibility, biological properties, and low immunogenicity *in vivo* [18].

### 1.5.3 Signals





Mesenchymal stem cells and preadipocyte cells could differentiate into adipocytes through many kinds of signal induction. Insulin, thyroid hormone, and dexamethasone, which is used to stimulate the glucocorticoid receptor pathway [33-35]; Isobutylmethylxanthine (IBMX), a phosphodiesterase inhibitor that has a protective effect on cAMP, has been used widely for the adipogenic agent [36]. In short summary, the signals that affect the adipogenic differentiation could be concluded with some properties in common, such as steroid-like structure, glucocorticoid, hormones, affect cAMP activity, and so on [37].

### **1.6 Purpose of the study**

The three major elements of tissue engineering are cells, scaffold, and signals. Although many tissue engineering technologies have been proposed for breast reconstruction, those technologies might match some of the goals but be still far away from the clinical requirements and patient's expectations. The purpose of this study is to develop the injectable engineered fat as a good environment for the cells toward the desired pathway. The injectable materials belong to a minimum invasive approach for breast reconstruction. Encapsulation of cells and bioactive molecules into the materials can enhance angiogenesis and cell survival rate *in vivo* for breast reconstruction after lumpectomy. The strategy of this study schemes in Fig.1.2.

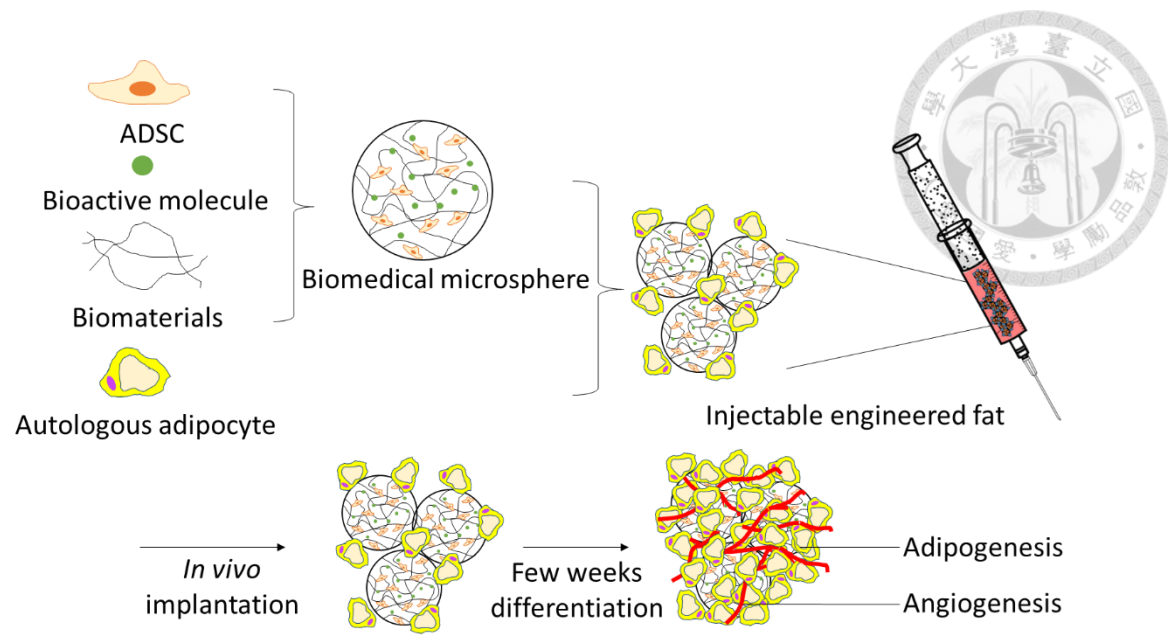


**Fig.1.2** The strategy of this study.

## Chapter 2 THEORETICAL BASIS



### 2.1 Alginate

Alginate is a biodegradable polymer that cells can be encapsulated to form an injectable hydrogel, beads, and the preformed scaffolds [4, 38, 39]. The chemical structure of alginate and the mechanism of alginate gel formation in the presence of divalent cations are shown in Fig.2.1. Although lack domains for cell recognition, alginate could graft some of the molecules to improve the cell adhesion, proliferation, and toward desired differentiation [39].

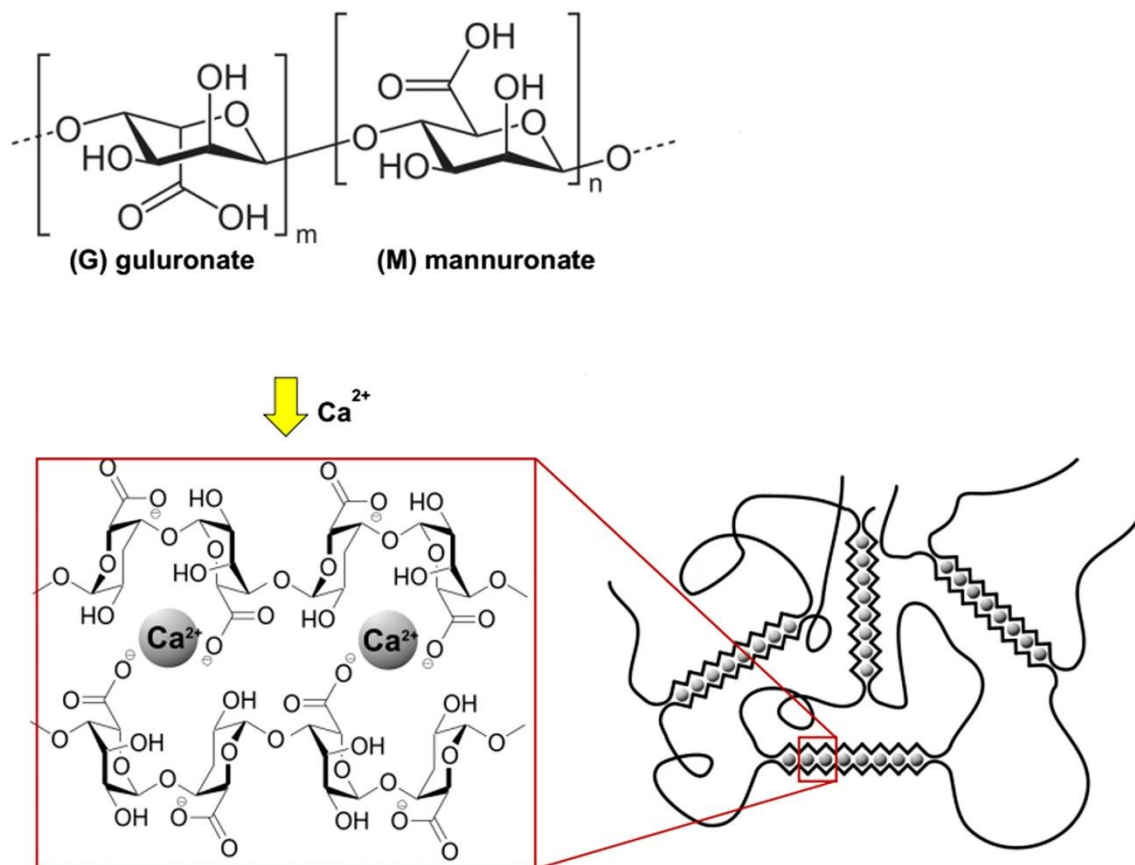
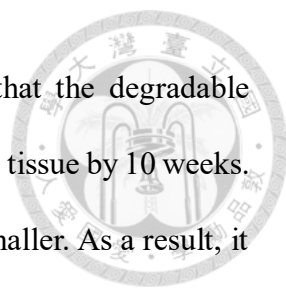


**Fig.2.1** Chemical structure of alginate and the mechanism of alginate gel formation in the presence of divalent cations [40].

The potential capacity of oxidized alginate hydrogels for adipose tissue engineering has been evaluated. Cell-loaded alginate hydrogels and cell suspensions were tested in a



nude mouse model injected subcutaneously. The results showed that the degradable alginate gel allowed capillaries to form in the newly generated adipose tissue by 10 weeks. Compared with the free cell control group, the volume loss is also smaller. As a result, it was confirmed that the injectable alginate hydrogel provides a suitable delivery vehicle for human adipose-derived stem cells. [32].

## 2.2 Laminin

Laminin, one of the major extracellular matrix glycoproteins, was first found intracellularly in the morula stage [41]. It has been shown to play an important role in early embryonic cell polarization and influence cell differentiation, migration, and adhesion [42, 43]. A laminin-modified biomaterial could influence cell adhesion and proliferation in the scaffold for several days [44-46] The structure of laminin is shown in Fig.2.2.

Sodium periodate ( $\text{NaIO}_4$ ) is widely used in chemical reactions due to its ability to act as an oxidant. Sodium periodate can oxidize two adjacent secondary hydroxyl groups, breaking the carbon-carbon bond and forming two aldehyde groups. These reactive aldehyde groups can be coupled to amine- or hydrazide-containing molecules via Schiff base reactions [47]. These reactions are commonly used to oxidize carbohydrates to generate reactive sites for subsequent incorporation of amine-containing molecules for polymer modification and bioconjugation [48-50].

In the study, we used a relatively low concentration of sodium periodate ( $\text{NaIO}_4$ ) by long reaction time to synthesize laminin-modified alginate to prepare a scaffold to mimic the embryonic environment. The chemical reaction to synthesis of laminin-modified alginate is shown in Fig.2.3.

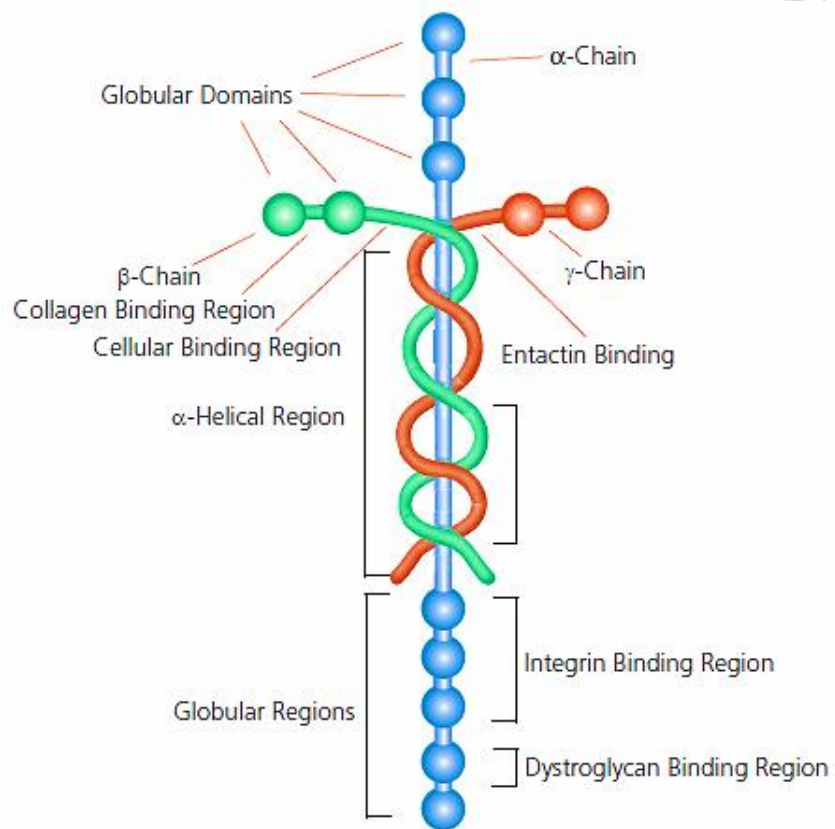


**Fig.2.2** Structure of laminin [51].



receptor and activating heat shock protein 90, ultimately enhancing the activity of nitric oxide synthase (NOS) [55-57]. The structure of ginsenoside Rg1 and the mechanism by which it induces angiogenesis are illustrated in Fig.2.4 and Fig.2.5, respectively. Nitric oxide plays a crucial role in mediating angiogenesis and the proliferation of endothelial cells [55, 58]. Rg1 has been reported as a non-peptide bioactive molecule capable of inducing mild angiogenesis with long-lasting stability in the physiological environment. Unlike protein-based growth factors, the bioactivity of Rg1 is not significantly affected by temperature, pH, or solvents [59, 60]. These properties make Rg1 a promising candidate for promoting angiogenesis in tissue engineering, as it offers a longer biostability compared to protein-based growth factors.

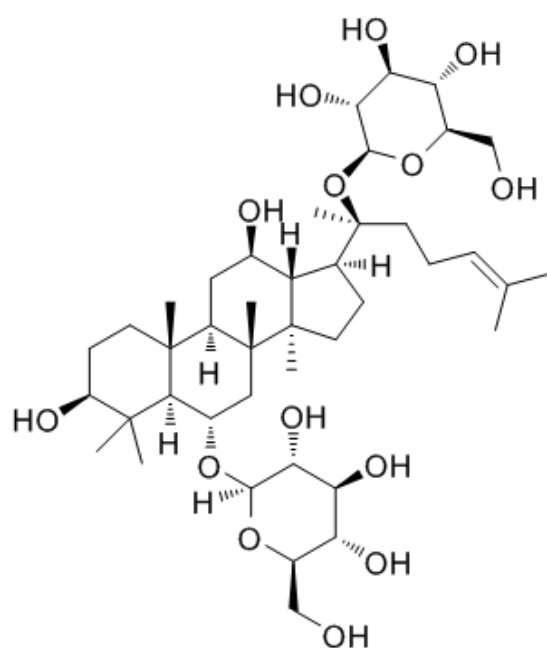


**Fig.2.4** Structure of the ginsenoside Rg1

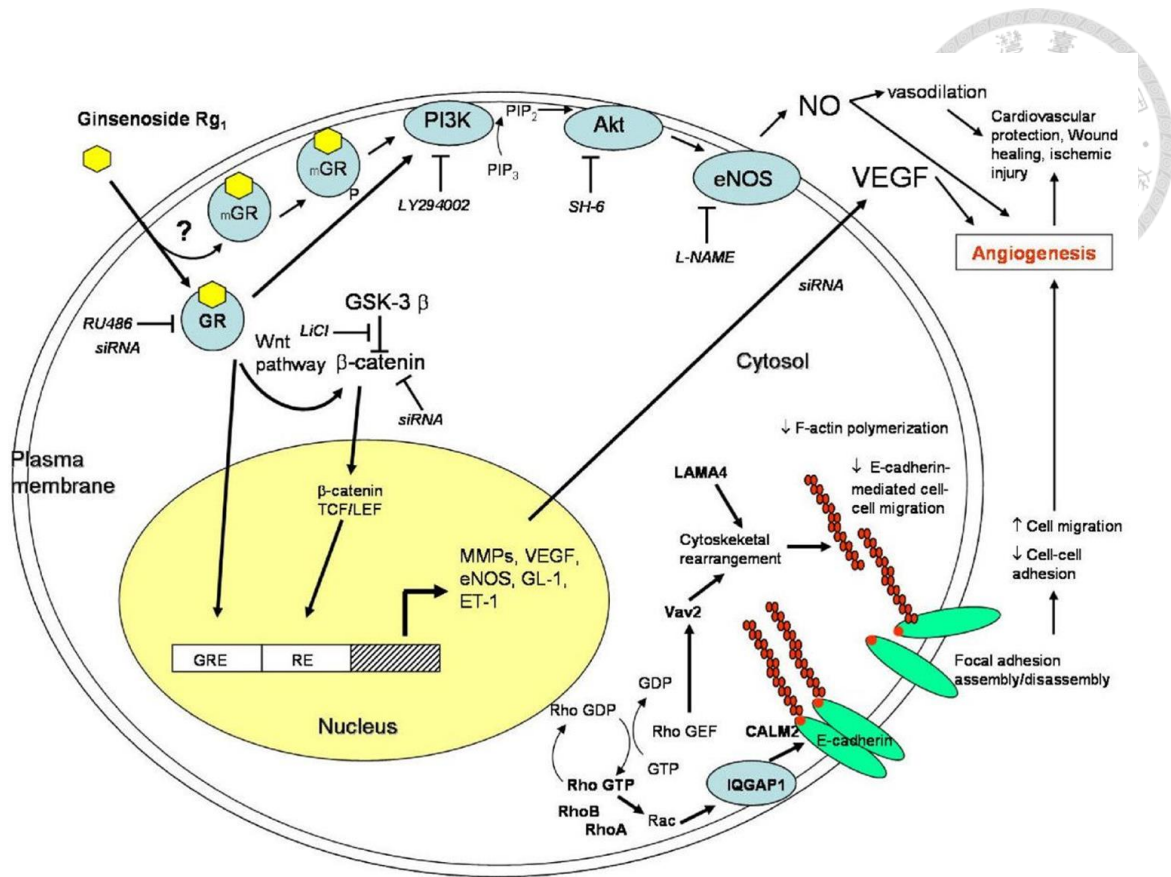


Fig.2.5 Rg1-mediated angiogenic mechanism in HUVEC [57].

## 2.4 Cells

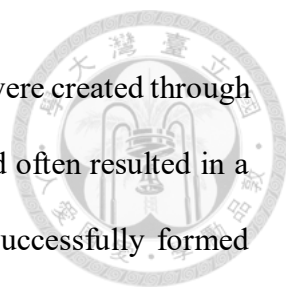
In the study, the adipose-derived stem cells (ADSCs) would be used as cell sources for the research, because ADSCs could differentiate into adipocytes, chondrocytes, myocytes, endothelial cells, osteoblasts under specific signals induction [4, 19].

The second cell source used in this study was adipocytes. The adipocytes could be isolated from the inguinal white adipose tissue [61]. The adipose tissue was considered to release a wide range of signals, inclusive of endocrine, autocrine, or paracrine [62, 63]. These secreted factors have been thought to trigger the differentiation of stem cells to adipocytes [64, 65].

## 2.5 Bio-electrospray method

The use of micron-sized beads as cell carriers has been shown to have benefits in terms of enhancing cell proliferation and survival rates due to the reduced diffusion rate





of nutrients, oxygen, and waste [28, 66]. Traditionally, microcarriers were created through emulsification caused by mechanical or shear forces, but this method often resulted in a non-uniform size distribution. In contrast, some researchers have successfully formed microcarriers by applying a consistent force, such as an electric field or hydrodynamic focusing, to disrupt the discontinuous phase [28, 67, 68]. The uniform size of the microspheres offers advantages in terms of promoting cell proliferation, survival, and optimizing the surface-to-volume ratio through homogeneous distribution [69-71].

Electrospray is a method of atomizing liquid with electricity. In the electrospray systems, upon different voltages, flow rate, fluid viscosity, and needle size would cause the different electrospray modes, inclusive of the dripping mode, cone-jet mode, oscillating mode, spindle mode, multijet mode, and so on (Fig.2.6) [72]. The liquid aerosol can be formed by electrostatic charging and may be used in different fields, such as the food and pharmaceutical industry [72]. The most stable mode of the electrospray system would be cone-jet mode, where the Taylor cone would form from the tip of the needle. The concept of the Taylor cone is shown in Fig.2.7.

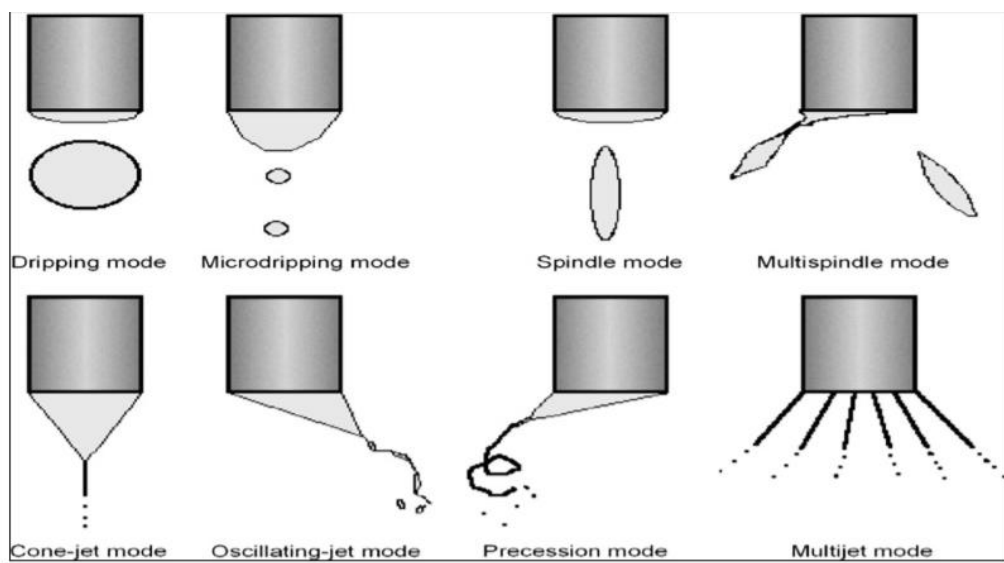


**Fig.2.6** Various modes of electrospray [72].

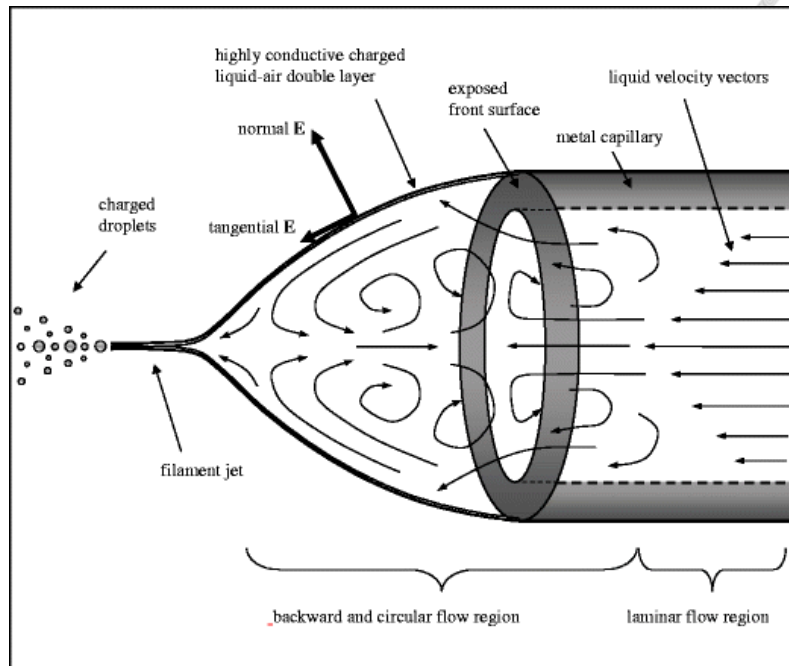


**Fig.2.7** Taylor cone and related concepts [73].

The bio-electro spray method is one technology that sprays a suspension of living cells to the collecting device. Upon defined condition, there the cells could be formed to the micro-droplet without damaging the cells [74]. In this study, we design a simple bio-electrospray system, shown in Fig.2.8. Spraying the cells and materials to the collecting device, forming the microspheres could be used in adipose tissue engineering.

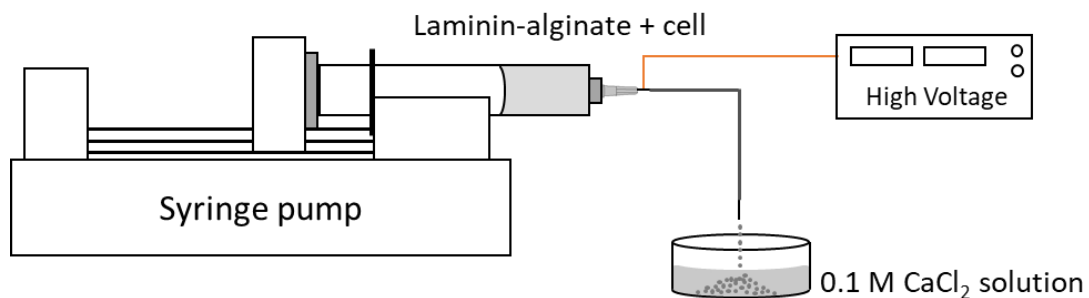
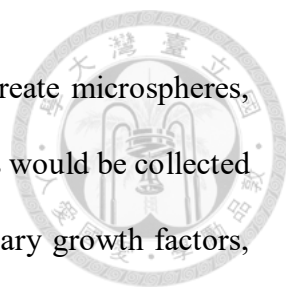


**Fig.2.8** Bio-electrospray system in the study.

## 2.6 Materials design of the study

In the work, the laminin-modified alginate, along with ADSCs and Rg1, would be mixed in a medium. This mixture would then be sprayed into a calcium chloride ( $\text{CaCl}_2$ )



solution using a power syringe and bio-electrospray technique to create microspheres, referred to as ADSC-G-LAMS. These ADSC-G-LAMS microspheres would be collected and combined with adipocytes to facilitate the production of necessary growth factors, directing the ADSCs towards the adipogenic pathway. The ADSC-G-LAMS microspheres and adipocytes would be combined and prepared in an injectable form for breast reconstruction. The overall design scheme is depicted in Fig.2.9.

The developed Rg1 loaded laminin-modified alginate microspheres (G-LAMS) would be characterized by Fourier transform infrared spectrophotometer (FTIR), optical microscope, scanning electron microscope (SEM) for functional groups identification, sphere size measurement, and microstructure examination, respectively. The high-performance liquid chromatography (HPLC) was used to evaluate the release profile of Rg1 from the G-LAMS microspheres. The HUVEC tube formation assay by Matrigel<sup>TM</sup> was used to evaluate the ability of vascularization of the developed G-LAMS microspheres. The cell viability, cytotoxicity, and genotoxicity were evaluated by WST-1, live/dead staining, and chromosome aberration, respectively, to confirm the safety of the designed G-LAMS. Gene expression of PI3K, Akt, and eNOs was determined by real-time quantitative PCR (Q-PCR) analysis to check the angiogenic ability of G-LAMS microspheres. The adipocytes and microspheres were combined as the injectable form for *in vivo* study by SD rats. The efficacy was investigated by hematoxylin & eosin (H&E) and immunofluorescence staining. The blood element analysis and serological analysis were used to evaluate the safety of the developed combination of adipocytes and ADSC-G-LAMS microspheres.

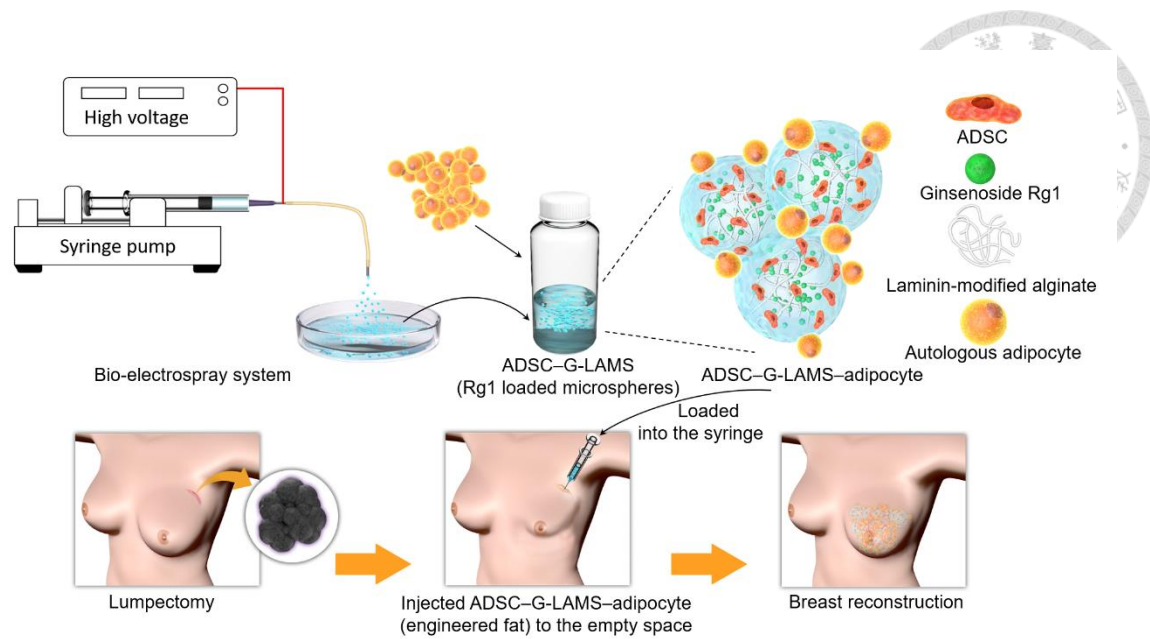


**Fig.2.9** Scheme illustration of ADSC-G-LAMS preparation and its applications on adipose tissue regeneration.

## Chapter 3 MATERIALS AND METHODS



### 3.1 Experimental instruments

The instruments and manufacturers used in this research are listed in Table 3.1.

**Table 3.1** Experimental instrument, manufacturers, and model

<b>Experimental Instruments</b>	<b>Manufacturers</b>	<b>Model</b>
Confocal microscope	Leica, Wetzlar, Germany	TCS SP8
Real-time PCR	Roche, Basel, Switzerland	LightCycler ® 96
Incubator	Thermo Scientific, Waltham, MA, USA	FV300
SEM	Hitachi, Tokyo, Japan	S-4800
FTIR	Jasco, Tokyo, Japan	FT/IR-4200
NMR	Bruker, Rheinstetten, Germany	AVIII-500
Centrifuge	Eppendorf, Hamburg, Germany	5804 R
pH meter	Microcomputer, San Diego, CA, USA	6171
Syringe pump	KD Scientific, New Hope, PA, USA	KDS 250
Voltage generator	Cosmi, New Taipei City, Taiwan	C-PME25
Freeze dryer	EYELA, Tokyo, Japan	FDU-1200

### 3.2 Experimental chemicals

The chemicals used in this research are shown in Table 3.2.

**Table 3.2** Experimental chemicals.



Chemicals	Product number	Company
Alginic acid sodium salt	A2158	Sigma
Calcium Chloride, Anhydrous	1311-01	J.T. Baker
HEPES Free Acid	4018-04	J.T. Baker
Ginsenoside Rg1	ASB-00007221	ChromaDex
Natural mouse laminin	354232	Corning
Matrigel	356231	Corning
Dulbecco's modified Eagle's medium -High glucose	D5648	Sigma
Medium 199	31100-035	gibco
Nutrient Mixture F-12 Ham	N3520	Sigma
Endothelial cell growth supplement from bovine neural tissue	E2759	Sigma
Fetal bovine serum	Characterized	Hyclone
Primocin™	ant-pm-2	Invivogen
Trypsin-EDTA	15400054	Gibco
Phosphate buffered saline	P4417	Sigma
LIVE/DEAD Cell Viability Assay	L3224	Thermo
TRIzol reagent	15596026	Thermo
Direct-zol RNA kit	R2052	Zymo
SuperScript III reverse transcription kit	18080-051	Thermo
SYBR Green Master Mix	K0252	Thermo
WST-1 Cell proliferation assay	MK400	Takara

Zinc diethyldithiocarbamate	329703	Sigma
Aluminum oxide	11028	Sigma
Sodium bicarbonate	S5761	Sigma
Dimethyl Sulfoxide	D2650	Sigma
Deuterium oxide	151882	Sigma
Wright-Giemsa Stain, Modified	WG16	Sigma
Methyl alcohol	32213	Sigma
Ethanol	32221	Sigma
Acetic acid	32209	Sigma
Paraformaldehyde	43368	Thermo
Acetonitrile, HPLC	915280	J.T. Baker
Demecolcine	D7385	Sigma

### 3.3 Flow chart of the study

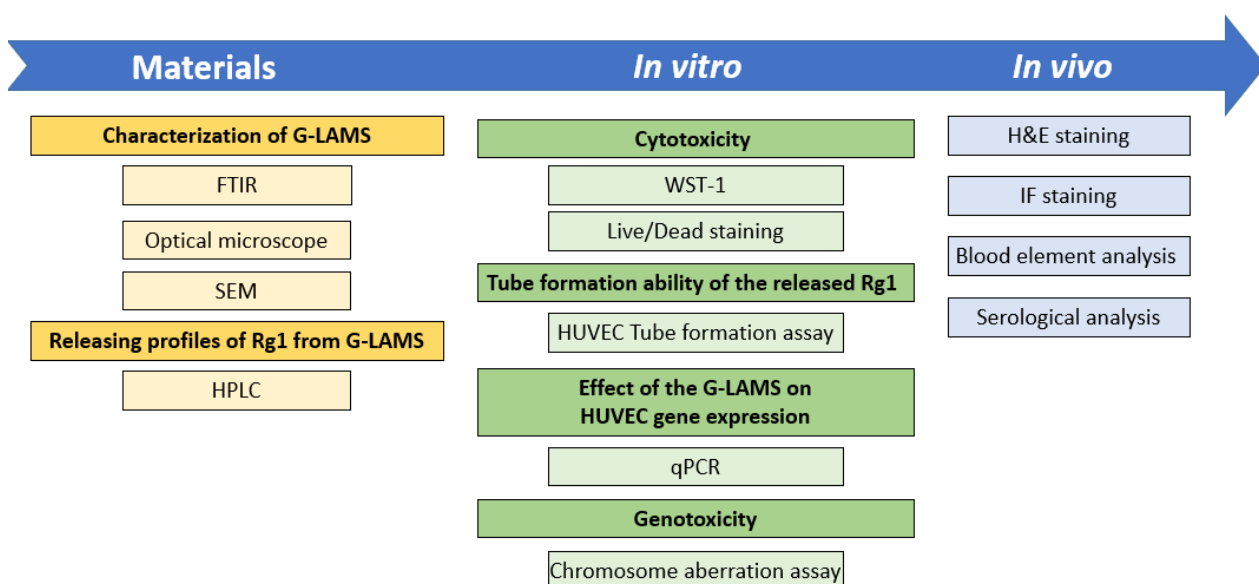
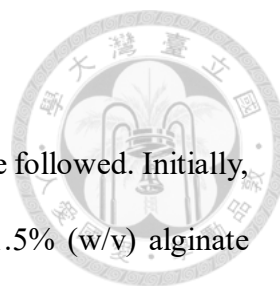


**Fig.3.1** Flow chart of the study.



### **3.4 The synthesis of laminin-modified alginate**

To prepare the laminin alginate solution, the following steps were followed. Initially, 0.5 mL of a 100 mM NaIO<sub>4</sub> solution was added to 100 mL of a 1.5% (w/v) alginate solution. The mixture was stirred at room temperature in the dark for 5 hours. Subsequently, 0.5 mL of ethylene glycol was added to stop the reaction. The resulting solution was then dialyzed against deionized water using a dialysis membrane (Cellu Sep, 8015-40, USA, MWCO: 6000-8000 Da) for a duration of 3 days, with the deionized water being replaced every 12 hours. After dialysis, the solution was freeze-dried (lyophilized) to obtain oxidized alginate powder. Next, 1.5 g of the obtained oxidized alginate powder was dissolved in 100 mL of a 20 mM 4-(2-hydroxyethyl)-1-piperazineethanesulfonic acid (HEPES) solution. Subsequently, 10 µg of laminin was added to the solution, completing the synthesis of the laminin-modified alginate.

### **3.5 The preparation of laminin-modified alginate microsphere (LAMS)**

To prepare the laminin-modified alginate microspheres, the bio-electrospray method was utilized. The setup of the bio-electrospray system involved three components: a syringe pump, a high voltage generator, and a collecting tank containing a 0.1 M CaCl<sub>2</sub> solution. First, 10 mL of the laminin-modified alginate solution was loaded into the syringe. The collecting tank was gently stirred. The syringe pump was set to a flow rate of 0.03 mL/min, and a low working voltage of 18 kV was applied using the high voltage generator. The distance between the syringe needle and the collecting tank was maintained at 1.5 cm, and the inner diameter of the needle was 500 µm. The laminin-modified alginate solution was then sprayed from the syringe needle into the collecting tank. During this process, gentle stirring of the collecting tank was continued. After the



spray process, the resulting microspheres were washed three times using 20 mM HEPES solution. The microspheres were then collected and prepared for subsequent experiments.

### **3.6 The preparation of Rg1 encapsulated in LAMS microsphere (G-LAMS)**

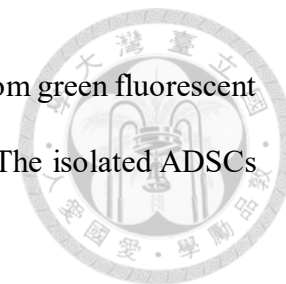
To prepare the G-LAMS microspheres, the Rg1 (at a concentration of 400 µg/mL) was encapsulated into the previously prepared LAMS microspheres (as described in Section 3.5). Specifically, 10 mL of the Rg1 solution was added to 10 mL of the LAMS microsphere solution. The mixture was then incubated at 37°C for 24 hours, allowing the Rg1 to penetrate and become encapsulated within the microspheres.

### **3.7 The preparation of ADSC-G-LAMS microsphere**

The ADSC-G-LAMS refers to the combination of laminin-modified alginate with ADSCs and Rg1, which is then transformed into microspheres using the bio-electrospray method as previously described in Section 3.5. To isolate the ADSCs, 5-week-old female Sprague-Dawley rats obtained from BioLASCO, Taiwan [75, 76] were used.

The inguinal fat was surgically removed and fragmented with surgical scissors. The fragmented fat tissue was washed with phosphate-buffered saline (PBS) and dissociated using type I collagenase (Invitrogen, USA) at 37°C for 4 hours. The cell suspension was then filtered through a 70-µm strainer and centrifuged at 1000 rpm for 5 minutes. The resulting cell pellets were collected and washed twice with PBS. The cells were cultured in a petri dish at a density of 5000 cells/cm<sup>2</sup> in DMEM with 10% FBS and 1% antibiotic-antimycotic and incubated overnight at 37°C in a humidified incubator. After 24 hours, non-adherent cells were removed, and the dish was rinsed twice with PBS. The medium was changed every 3 days until the cells reached confluence. ADSCs from passages 3-5 were used for subsequent experiments. ADSCs  $2 \times 10^7$  were suspended in 10 mL laminin-modified alginate solution, and the microspheres were prepared by the bio-electrospray

as described above. For the *in vivo* study, the ADSCs were isolated from green fluorescent protein transgenic (GFP) 7-week-old female Sprague-Dawley rats. The isolated ADSCs with GFP were abbreviated as GFP-ADSCs.



For the preparation of ADSC-G-LAMS microspheres,  $2 \times 10^7$  ADSCs were suspended in 10 mL of the laminin-modified alginate solution. The microspheres were then prepared using the bio-electrospray method as described earlier. For the *in vivo* study, the ADSCs were isolated from green fluorescent protein transgenic (GFP) 7-week-old female Sprague-Dawley rats. These isolated ADSCs, which expressed GFP, were referred to as GFP-ADSCs.

### **3.8 The analysis of Fourier transform infrared spectrophotometer (FTIR)**

An FTIR spectrophotometer (Jasco, FT/IR-4200, Japan) was used to identify the functional groups of laminin-modified alginate. Freeze-dried samples were mixed with KBr by the weight ratio of 1:9 and then placed in an aluminum ring to press into a disc by gentle pressure. The FTIR pattern was obtained by transmission mode with 16 scans from  $4000 \text{ cm}^{-1}$  to  $600 \text{ cm}^{-1}$ .

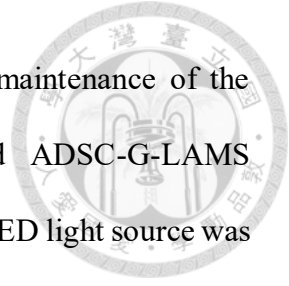
### **3.9 The analysis of nuclear magnetic resonance (NMR)**

$^1\text{H}$  NMR spectra were recorded on a Bruker Avance III 500 Spectrometer operating at a 500MHz superconducting magnet for a magnetic field of 11.75 Tesla at ambient temperature. 8 mg of each sample was dissolved in 0.8 ml of  $\text{D}_2\text{O}$ . After filtering the resultant solution with a 0.22 filter, the sample was added to the NMR tube for detection.

### **3.10 The size measurement and morphology observation of the developed ADSC-G-LAMS microspheres**

The ADSC-G-LAMS microspheres were cultured in DMEM supplemented with 10% FBS and 0.1% Primocin antibiotic (Invivogen, San Diego, CA). The culture medium

provided the necessary nutrients and support for the growth and maintenance of the microspheres. To observe the morphology of the developed ADSC-G-LAMS microspheres, an optical microscope equipped with a high-intensity LED light source was used. This enhanced brightness allowed for better visualization of the microsphere structures. The size of the ADSC-G-LAMS microspheres was measured using ImageJ software. At least 50 microspheres were imaged and counted under the optical microscope.



### **3.11 The SEM examination of the ADSC-G-LAMS microspheres**

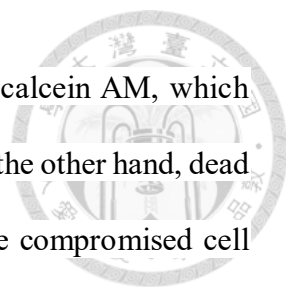
On day 5 of culturing the ADSC-G-LAMS in the petri dish. The ADSC-G-LAMS microspheres were washed with HEPES buffer twice and then collected. The collected microspheres were immersed step-by-step in the series dehydration and followed by a critical point dryer (CPD). The CPD dried microspheres were mounted on an Al-stage and then coated with a platinum film by sputtering PVD. The ADSC-G-LAMS microspheres were examined under the scanning electron microscope (S-4800, Hitachi, Japan) for microstructure examination.

### **3.12 Cytotoxicity of the G-LAMS microsphere**

The cell viability of the G-LAMS was evaluated using a WST-1 assay. G-LAMS was soaked into the medium for 24 hours, and the extracts were cultured with 3T3-L1 fibroblast for cell viability test; that would be in terms of cytotoxicity of the developed G-LAMS microsphere-based on the ISO-10993 guideline. Each group was 4 repeats.

### **3.13 ADSCs viability in the ADSC-G-LAMS microspheres**

To assess the viability of ADSCs within the G-LAMS microspheres, a live/dead staining assay was performed. On both day 1 and day 5 after ADSCs were encapsulated in G-LAMS (ADSC-G-LAMS), the microspheres were gently washed twice. Subsequently, the microspheres were stained with specific dyes in the dark at 37°C for 1



hour. In the live/dead staining assay, living cells were stained with calcein AM, which produces a green fluorescence upon intracellular esterase activity. On the other hand, dead cells were stained with ethidium homodimer-1, which penetrates the compromised cell membranes of dead cells and emits red fluorescence when bound to nucleic acids. After staining, the microspheres with the encapsulated ADSCs were mounted on a glass slide and observed under a fluorescent microscope.

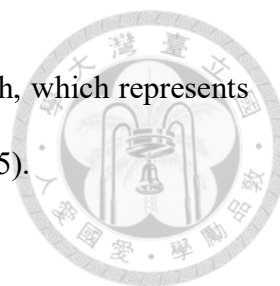
### **3.14 Releasing profiles of Rg1 from G-LAMS**

The releasing profiles of Rg1 from G-LAMS were recorded by high-performance liquid chromatography (HPLC). G-LAMS were placed into the deionized water at 37°C (n = 3) for a period and then taken out for centrifugation. The supernatant was collected before injection into the HPLC system.

All the samples were filtered with a 0.22 µm filter before injection. The C18 HPLC column (XBridge BEH C18 Method Validation Kit, 130Å, 5 µm, 4.6 mm X 250 mm, 186003776) was run at a flow rate of 1 mL/min under UV detector at 203 nm. The mobile phase consisted of 30% acetonitrile and 70% ddH<sub>2</sub>O. The injection volume was 10 µL.

### **3.15 The tube formation ability of the released Rg1**

To evaluate the tube formation ability of the released Rg1, human umbilical vein endothelial cells (HUVECs) were used as a model for angiogenesis. A 96-well plate was coated with 50 µL of Matrigel. HUVECs were seeded at a density of  $1 \times 10^4$  cells per well in 150 µL of medium 199 (M199) supplemented with 2% FBS and the released Rg1. The medium with 2% FBS alone served as the blank control, while the medium with 2% FBS and endothelial cell growth supplement (30 µg/mL ECGS) was used as the positive control. After incubation for 6 hours, images of the formed tubes were captured using an optical microscope. These images were then converted into grayscale and analyzed using



the angiogenesis analyzer plugin in ImageJ software. The tube length, which represents the extent of tube formation, was quantified using this software (n = 5).

### 3.16 Effect of G-LAMS on HUVEC gene expression

Table 3.3.

In the experiment, HUVECs were seeded into each well of a 6-well plate at a density of  $1.67 \times 10^5$  cells per well and allowed to fully adhere for 24 hours. After that, the cells were starved by replacing the medium with M199 serum-free medium and incubated for an additional 4 hours. Subsequently, the medium was changed to 1.775 mL of M199 containing 2% FBS, and the experimental groups received the addition of LAMS or G-LAMS, while the control group received blank medium without any treatment. After an hour of treatment, the HUVECs were collected and washed twice with PBS. The cells were then lysed using TRIzol reagent (Thermo Fisher), and the supernatants were collected. Total RNA was extracted from the collected supernatants using the Direct-zol™ RNA MiniPrep Kits (Zymo Research, Irvine, CA, USA). The extracted RNA was subjected to reverse transcription using SuperScript™ III Reverse Transcriptase (Thermo Fisher) to obtain cDNA for real-time quantitative PCR (Q-PCR) analysis. The synthesized cDNA was mixed with SYBR Green Master Mix (Thermo Fisher), and the primers listed in Table 3.3. were used for the analysis. The intensity of the amplified products was detected and recorded using the LightCycler® 480 Instrument (Roche Diagnostics Nederland BV, Almere, Netherlands) (n = 3).

**Table 3.3** Primers for Real-time PCR.

Primer	Sequence (5' → 3')
GAPDH forward	ACCACAGTCCATGCCATCAC

GAPDH reverse	TCCACCACCCTGTTGCTGTA
PIK3CA forward	AACACTCAAAGAGTACCTTGTTCCAA
PIK3CA reverse	TAGCACCCCTTTCGGCCTTTA
PIK3R1 forward	GCGAGATGGCACTTTTCTTGT
PIK3R1 reverse	TACTTCGCCGTCCACCACTAC
AKT3 forward	CCTTCCAGACAAAAGACCGTTT
AKT 3 reverse	ATGTAGATAGTCCAAGGCAGAGACAA
AKT1 forward	CTTTGCCGGTATCGTGTGGC
AKT reverse	CTCGCTGTCCACACACTCCA
eNOs forward	GTGATGGCGAAGCGAGTGAAG
eNOs reverse	CCGAGCCCGAACACACAGAAC

### 3.17 To evaluate the genotoxicity of G-LAMS by chromosome aberration assay

$2 \times 10^5$  Chinese hamster ovary cells (CHO cells) were plated in a 10 cm petri dish for 20 hours. Later, 10 mL of G-LAMS extract was added as the experimental group and culture medium only was as the control group. At 18 hours after treatment, 200  $\mu$ L of colchicine 10  $\mu$ g/mL was added. At 20 hours, cells were trypsinized and collected in a centrifugation tube. 5 mL of 0.075 M KCl was added to the centrifugation tube and gently shaken. Leave the tubes at 37°C for 15 min to allow cells to be swelled and then fixed by 5 mL of fixation solution (methanol: acetic acid = 3:1) at 4°C for 20 min. The suspension was droplet to a glass slide by a force to break down the cells; the breakdown cells were then stained with 10% Giemsa for 15 min. Filtered the Giemsa stain with the filter paper (Advantec, Qualitative Filter Paper, NO.1, Japan) before use. A total of 70 breakdown metaphase cells were counted under the optical microscope. The sister chromosome

aberration was recorded. The P-value of the aberration frequency was analyzed by one-sided Fisher's exact test.

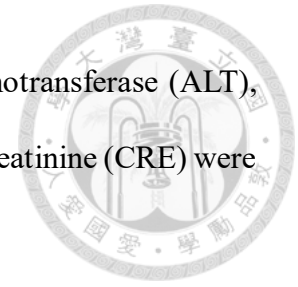


### **3.18 *In vivo* study**

The study involved a total of 12 Sprague-Dawley rats obtained from BioLASCO, Taiwan, with an average age of 6 weeks. The study protocol was approved by the Institutional Animal Care and Use Committee (IACUC) of Far Eastern Memorial Hospital under the approval number 2018-FEMH-11.

The rats were divided into three groups for the study. The first group involved the combination of GFP-ADSCs with shredded adipose tissue (abbreviated as ADSC-Adipocyte). The second group consisted of GFP-ADSCs encapsulated in 1 mL of laminin-alginate microspheres combined with shredded adipose tissue (abbreviated as ADSC-LAMS-Adipocyte). The third group included GFP-ADSCs and Rg1 encapsulated in 1 mL of laminin-alginate microspheres combined with shredded adipose tissue (abbreviated as ADSC-G-LAMS-Adipocyte). These groups were injected subcutaneously into the dorsum of the rats. After 4 weeks, the grafted tissues were harvested, fixed, embedded, and sectioned into 5  $\mu\text{m}$  thick slices, which were then placed on glass slides. The sections were stained with hematoxylin and eosin (H&E) to visualize tissue morphology and immunofluorescence staining for CD31 to assess blood vessel formation. The images of the sections were observed under an optical microscope and a confocal microscope to analyze the results. Furthermore, blood element analysis and serological analysis were conducted, including measurements of red blood cells (RBC), hemoglobin (HGB), hematocrit (HCT), mean corpuscular volume (MCV), mean corpuscular hemoglobin (MCH), mean corpuscular hemoglobin concentration (MCHC), white blood cells (WBC), neutrophils (NEUT), lymphocytes (LYMPH), monocytes (MONO),

eosinophils (EO), and basophils (BASO). Additionally, alanine aminotransferase (ALT), aspartate aminotransferase (AST), blood urea nitrogen (BUN), and creatinine (CRE) were analyzed in the serological analysis.



### 3.19 Statistics

Results are presented as the mean and standard deviation of at least three independent measurements. One-way ANOVA with Tukey's multiple comparisons test was used for all statistical evaluations except for one-sided Fisher's exact test for chromosome aberration assay. Differences were considered significant at a *p*-value of less than 0.05. ( $p < 0.05$ , \*;  $p < 0.01$ , \*\*;  $p < 0.001$ , \*\*\*).



## Chapter 4 RESULTS



### 4.1 FTIR functional groups analysis

The functional groups of the synthesized laminin-modified alginate were analyzed by Fourier transform infrared spectrophotometer (FTIR). The infrared spectra were recorded in the wavelength from 600  $\text{cm}^{-1}$  to 4000  $\text{cm}^{-1}$  (supplemental Fig.S1). The FTIR pattern of laminin-modified alginate prepared by relatively low concentration of sodium periodate and extended long reaction time was similar to the pattern synthesized by the previous method. The appearance of the absorption band at 1735  $\text{cm}^{-1}$  in laminin-alginate confirmed that forming of the aldehyde group (C=O), which indicated that oxidation had occurred. The absorption bands at 1600  $\text{cm}^{-1}$  and 1414  $\text{cm}^{-1}$  were corresponding to asymmetric and symmetric stretching vibrations of the carboxyl group, respectively, both shown in alginate and laminin-modified alginate. The absorption band at 1470  $\text{cm}^{-1}$  in the spectrum of laminin-modified alginate was attributed to the amide bond (N-H). The bands at 2850  $\text{cm}^{-1}$  and 2920  $\text{cm}^{-1}$  were assigned to asymmetric and symmetric C-H vibrations, respectively. The Schiff bases between 1631.5  $\text{cm}^{-1}$  and 1640.9  $\text{cm}^{-1}$  attributed to the C=N stretch characteristic of the imino group were not very clear due to strong absorption of the carboxyl group and low concentration of laminin.

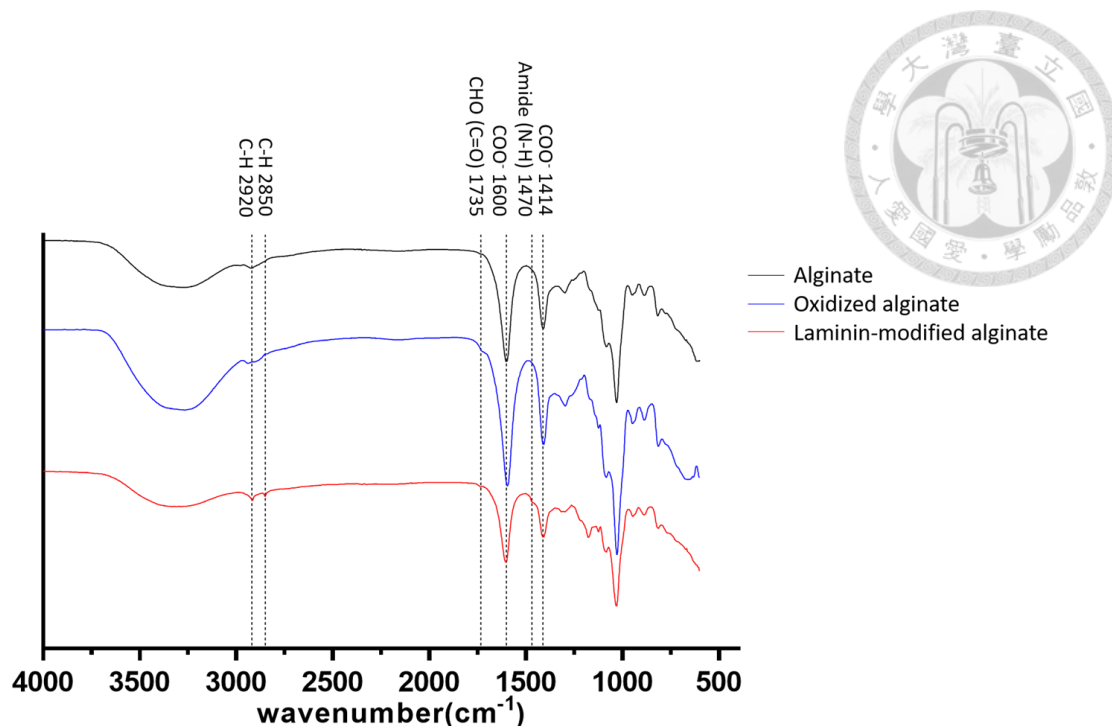


**Fig.4.1** The FTIR spectrum of alginate and laminin-modified alginate. The absorption band at  $1735\text{ cm}^{-1}$  confirmed that forming of aldehyde group (C=O). A new absorption band at  $1470\text{ cm}^{-1}$  in laminin-modified alginate indicates the amide bond formation. Furthermore, the band at  $2850\text{ cm}^{-1}$  and  $2920\text{ cm}^{-1}$  corresponded to asymmetric and symmetric C-H vibrations were also strengthened after modification.

#### 4.2 $^1\text{H}$ NMR spectrophotometry analysis

Furthermore, the  $^1\text{H}$  NMR spectra of alginate and laminin-modified alginate were applied to check the structure change, as shown in Fig.4.2. The peaks ranging from 3.66 to 4.99 ppm belonged to the protons of G and M units of the alginate peaks. The peaks ranged from 0 to 3 ppm which corresponded to the laminin signal [77]. Moreover, peaks that appeared at 5.08 ppm and 5.13 ppm corresponded to a hemiacetalic proton formed from aldehyde and hydroxy group but were not obvious in the laminin-modified alginate, owing to the low concentration of the sodium periodate and the complete reaction of the laminin modification [78].

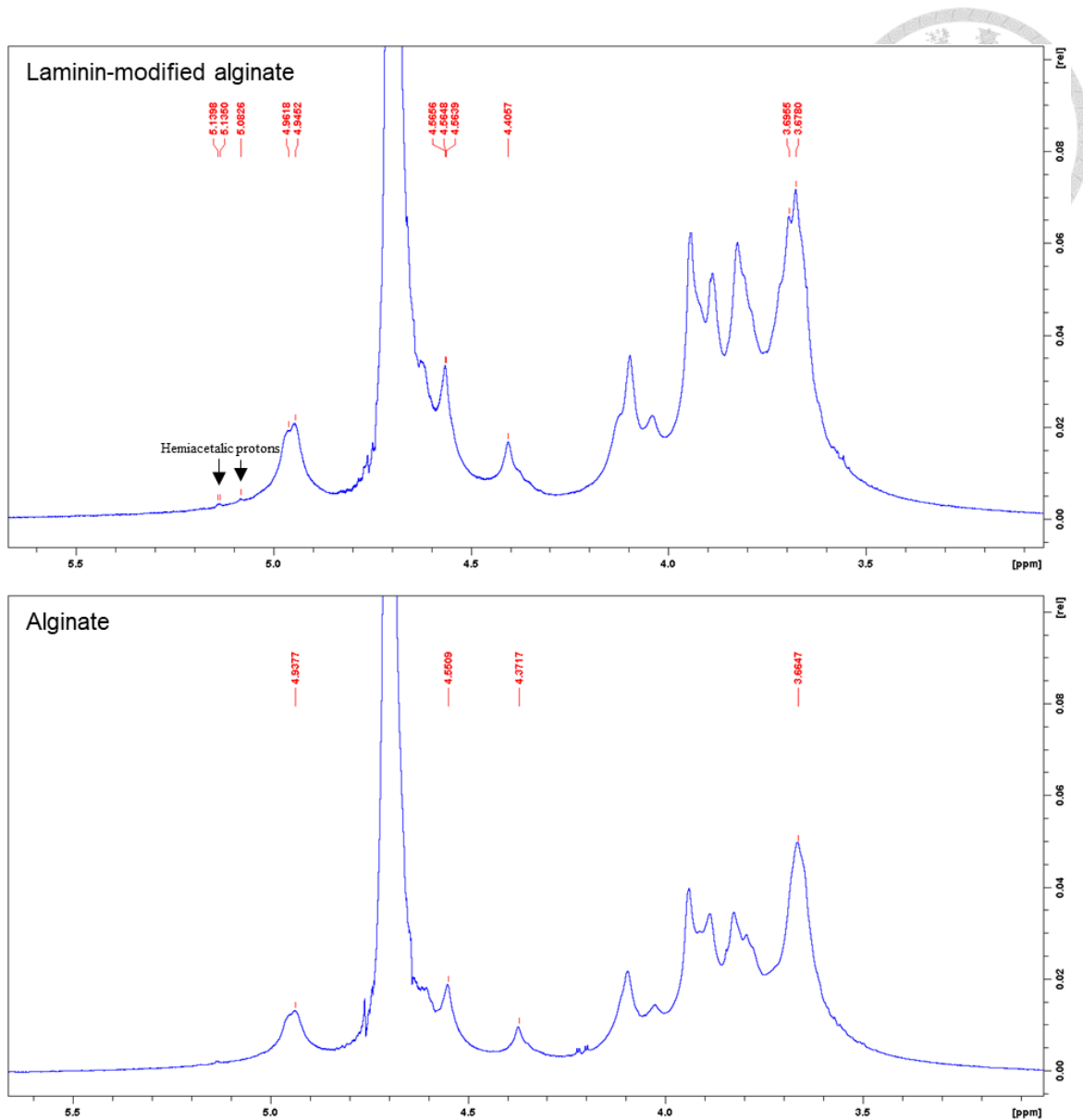


**Fig.4.2**  $^1\text{H}$  NMR spectrum of alginate and laminin-modified alginate. The peaks ranging from 3.66 to 4.99 ppm belonged to the protons of G and M units of the alginate peaks. Additional peaks appeared at 5.08 ppm and 5.13 ppm corresponded to a hemiacetalic proton formed from aldehyde and hydroxy group in the laminin-modified alginate.

### 4.3 The size measurement of the LAMS

The bio-electrospray device was constructed as shown in Fig.4.3 In the electrospray system, voltage and flow rate could be controlled to obtain different electrospray modes as shown in Fig.4.4. In this study, different parameters were firstly tested and found the

parameters which were the most stable and could form the microspheres with about 220  $\mu\text{m}$  in diameter (Fig.4.4(c)).

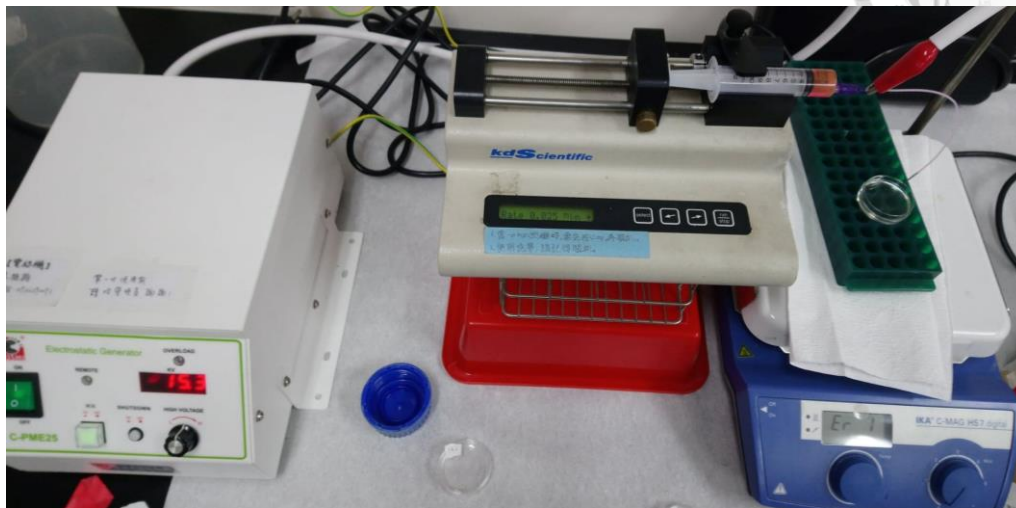


**Fig.4.3** Construction of the device of the bio-electrospray system.

<b>Voltage &amp; fluid flow rate</b>	8 kV & 0.008 mL/min	15 kV & 0.020 mL/min	15 kV & 0.030 mL/min
<b>size</b>	958.75 $\pm$ 80.91 $\mu\text{m}$	168.96 $\pm$ 23.14 $\mu\text{m}$	221.06 $\pm$ 24.25 $\mu\text{m}$

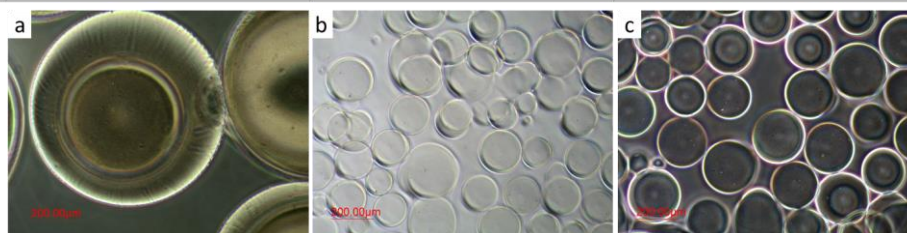


**Fig.4.4** Different sizes of the LAMS formed by different electro spray modes. (a) Microdripping mode, (b), (c) Cone-jet mode.

#### 4.4 The size measurement and SEM examination of the developed ADSC-G-LAMS microspheres

The ADSC-G-LAMS microspheres were prepared by the bio-electrospray with a power syringe as shown in Fig.4.5. The microspheres were very uniform in diameter with  $174.68 \pm 26.93 \mu\text{m}$  on average at day 0 as shown in Fig.4.5(a). The size of the spheres would be expanded to a mean value of  $232.42 \pm 42.37 \mu\text{m}$  at day 2, day 5, and day 9, as shown in Fig.4.5(b), Fig.4.5(c), and Fig.4.5(d), respectively, due to swelling. The ADSCs

were small white spots indicated as an arrow in the pictures, that was encapsulated in the microsphere homogeneously. The microspheres were further examined under SEM; where the ADSCs were fully embedded in the G-LAMS microspheres as shown in Fig.4.5(e) and Fig.4.5(f).

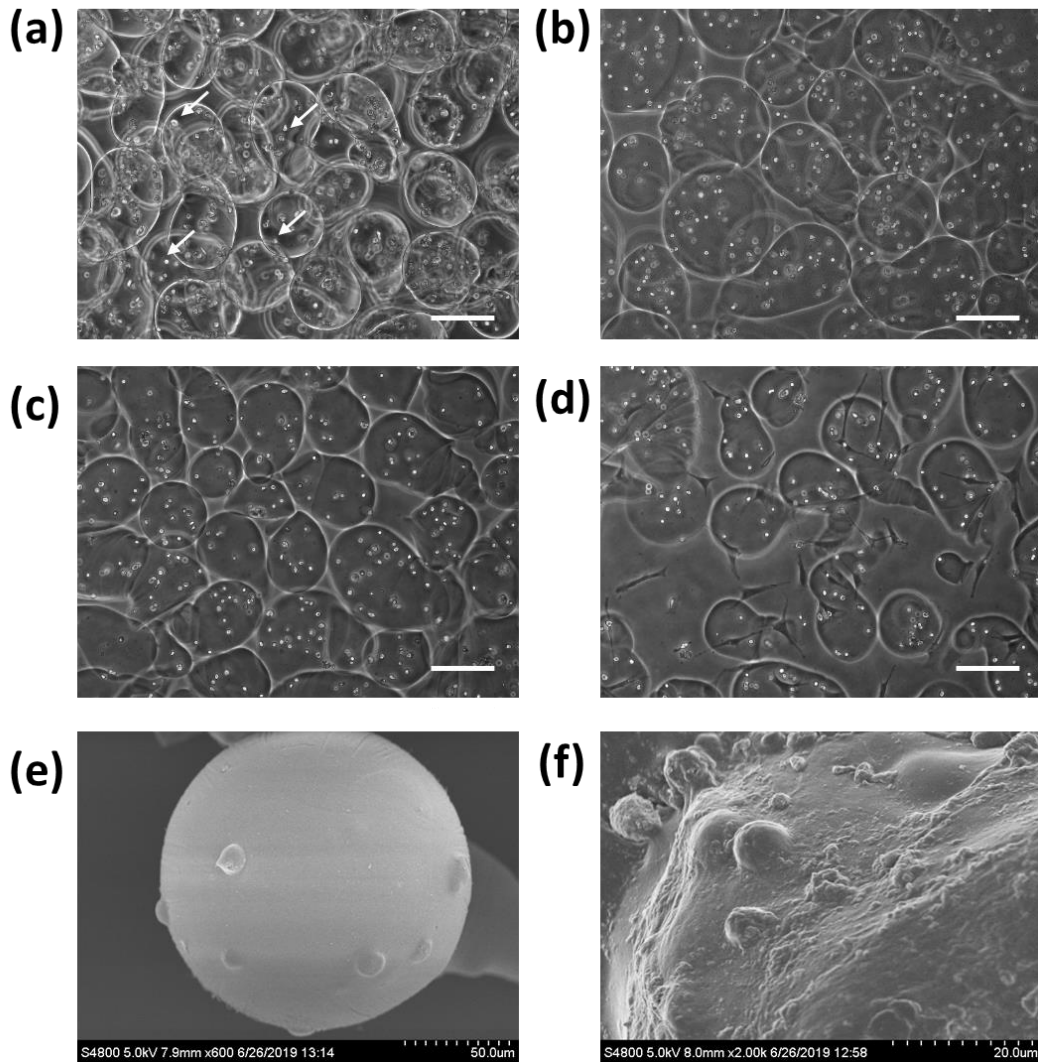
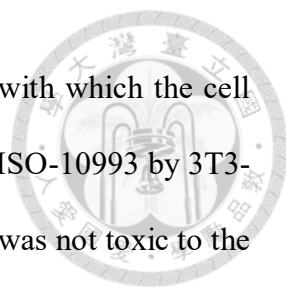


**Fig.4.5** Morphology and microstructure of laminin-alginate microspheres were observed by optical microscope and SEM. The image was taken by optical microscope at (a) Day 0, (b) Day 2, (c) Day 5, (d) Day 9 after ADSC-G-LAMS preparation. The arrows indicated the ADSCs encapsulated in G-LAMS. Scale bar = 200  $\mu\text{m}$ . SEM images were taken on Day 5 at (e) 600X magnification and (f) 2000X magnification.

#### 4.5 The cytotoxicity of G-LAMS

The cytotoxicity of G-LAMS was evaluated by WST-1 assay; with which the cell viability would be in terms of cytotoxicity based on the guidance of ISO-10993 by 3T3-L1 as target cells. The results showed that the synthesized G-LAMS was not toxic to the target cells, as shown in Fig.4.6.



The survival rate of ADSCs enclosed in G-LAMS was checked by live/dead staining assay (Fig.4.7). The living cells were stained with calcein AM and dead cells were stained with ethidium homodimer-1; which would turn into green and red, respectively, observed under the fluorescence microscope. As shown in Fig.4, more than 99% of ADSCs were alive in microspheres on day 1 and day 5. The cell number on day 5 (Fig.4.7(b)) was much high than that on day 1 (Fig.4.7(a)). We could tell that the developed G-LAMS was not toxic to the encapsulated ADSCs and created a good micro-environment for ADSCs proliferation.

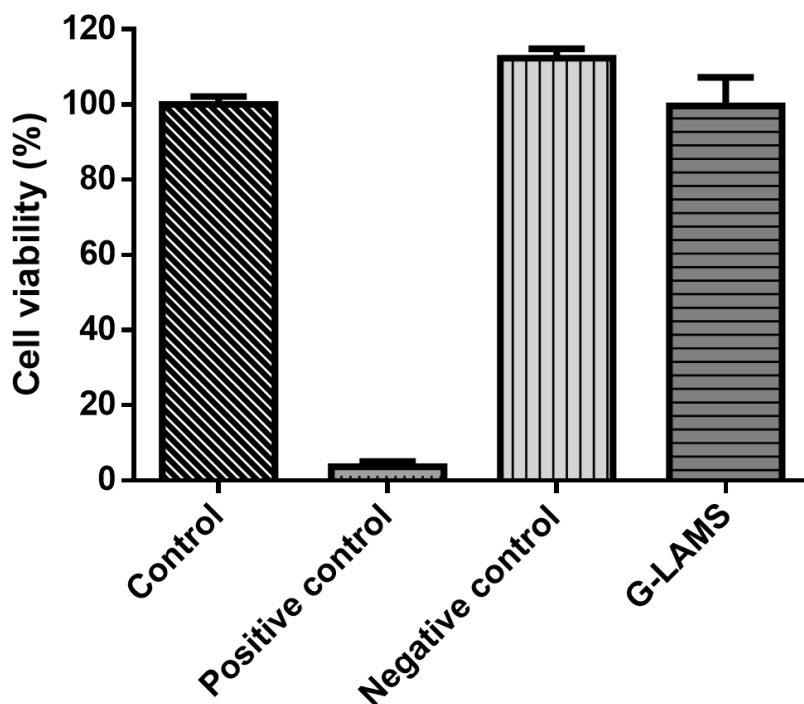
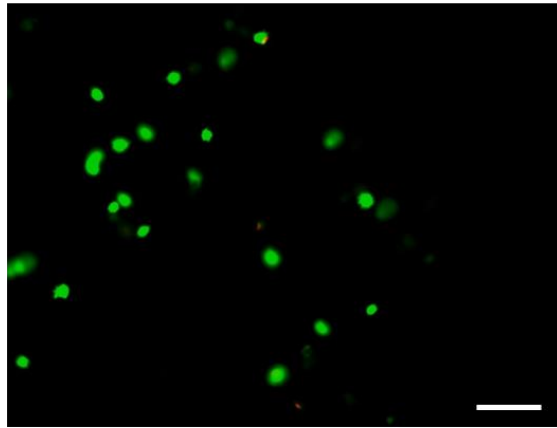


**Fig.4.6** The cell viability of G-LAMS was evaluated by 3T3-L1 viability based on the guidance of ISO-10993; the results would be in terms of cytotoxicity (n = 4).

(a)



(b)

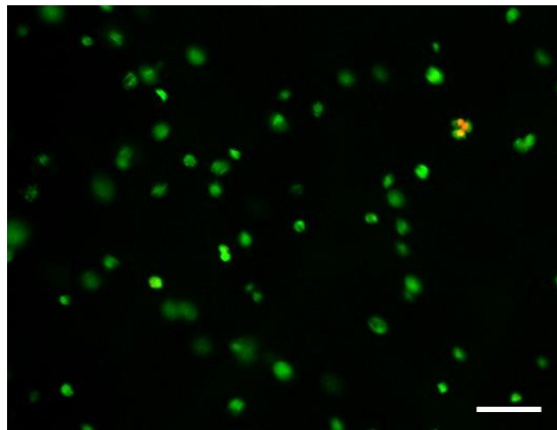


**Fig.4.7** ADSCs in ADSC-G-LAMS were evaluated by live/dead staining assay. ADSCs were encapsulated in G-LAMS and analyzed at (a) Day 1, and (b) Day 5. The living cells color in green were stained with calcein AM and dead cells color in red were stained with ethidium homodimer-1. Scale bar = 100  $\mu\text{m}$ .

#### **4.6 Releasing profiles of Rg1 from G-LAMS**

The cumulative Rg1 released from laminin-alginate microspheres is shown in Fig.4.8. The Rg1 release profile could be seen in two steps. The release rate at the first stage was 270  $\mu\text{g}/\text{day}$  which was due to physical desorption of Rg1 on the surface of the microsphere, as so-called initial burst. On the first day was about 67.4% released. The second stage was the relatively slow release of the Rg1 with the rate of 12  $\mu\text{g}/\text{day}$ , based on the diffusion process. Supposedly, the Rg1 would be fully released within 5 days.

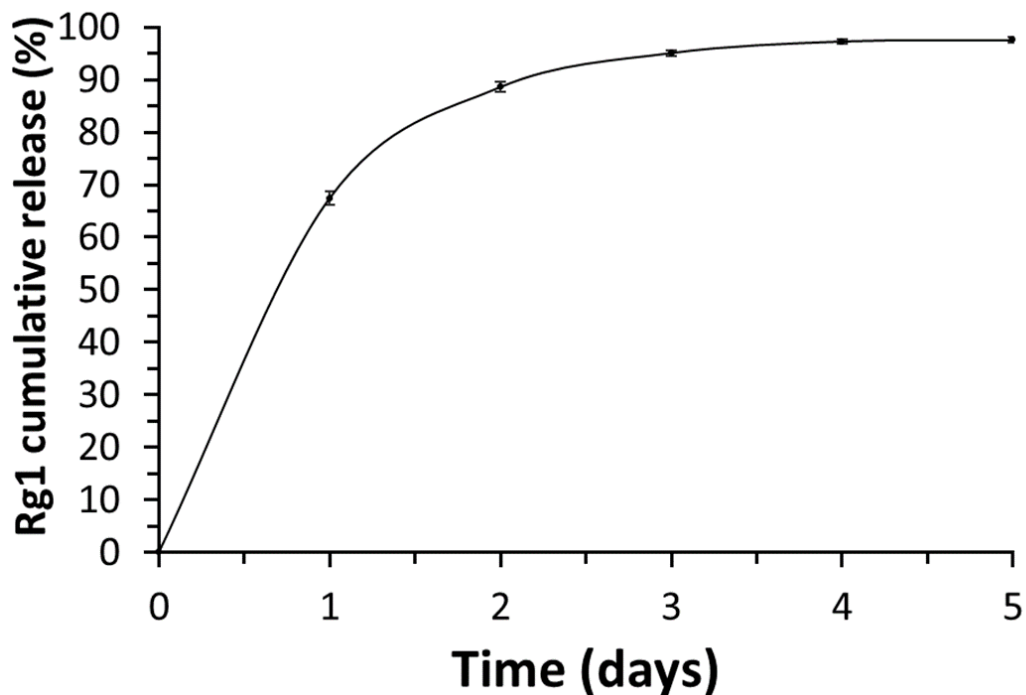


**Fig.4.8** Releasing profiles of Rg1 from G-LAMS. The cumulative Rg1 released curve was evaluated by HPLC analysis over time (n = 3).

#### **4.7 The ability of the tube formation for the synthesized G-LAMS**

The ability of the tube formation of the developed G-LAMS was determined by Matrigel<sup>TM</sup> and HUVEC. The experiment was divided into three groups: (1) control group: medium with 2% FBS (Fig.4.9(a)); (2) positive control: medium with 2% FBS and endothelial cell growth supplement (ECGS) (Fig.4.9(b)); (3) G-LAMS group: medium with 2% FBS and released Rg1 from G-LAMS without endothelial cell growth supplement (Fig.4.9(c)). The results were summarized in Fig.4.9(d); where the total tube lengths of the positive control and G-LAMS groups increased by 16.1% and 35.9%, respectively, compared to the control group. We believe that the Rg1 released from G-LAMS could keep biological activity to induce HUVEC cells vascularization by the Matrigel<sup>TM</sup> model.



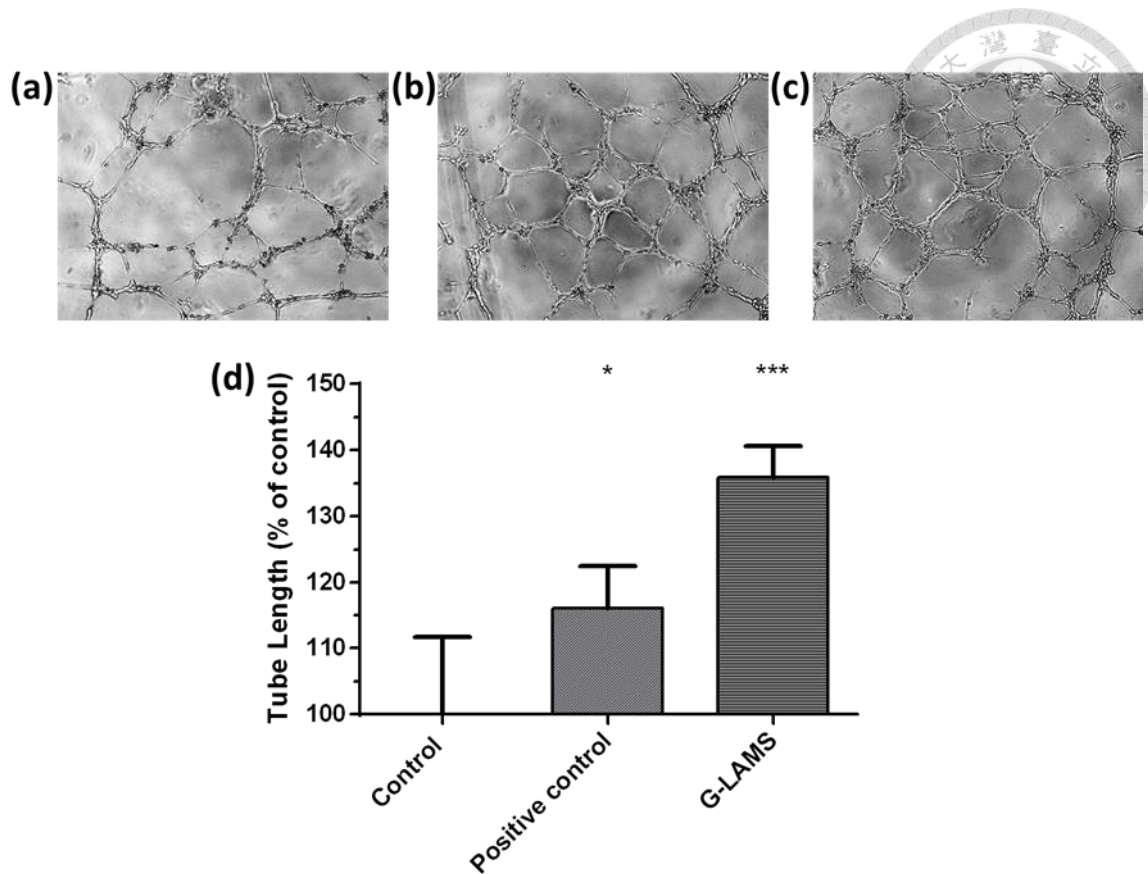


**Fig.4.9** The ability of the tube formation of the released Rg1 was tested by HUVEC tube formation assay with Matrigel™ (a) Control: medium with 2% FBS (b) Positive control: medium with 2% FBS and endothelial cell growth supplement (ECGS) (c) G-LAMS: medium with 2% FBS and released Rg1 from G-LAMS without ECGS. (d) Quantification by ImageJ software. ( $p < 0.05$ , \*;  $p < 0.001$ , \*\*\*, compared to control group by one-way ANOVA with Tukey's multiple comparisons test.)

#### 4.8 Effect of G-LAMS on HUVEC gene expression

To explore the role of the G-LAMS on HUVEC angiogenesis property, several genes such as PIK3CA (phosphatidylinositol 3'-kinase (PI3K) catalytic subunit p110 $\alpha$ ), PIK3R1 (PI3K regulatory subunit p85 $\alpha$ ), AKT3 (serine/threonine-protein kinase), eNOS (endothelial nitric oxide synthase) were measured by Q-PCR analysis. The results showed that the coculture of G-LAMS with HUVECs could affect the upstream genes, PIK3CA, PIK3R1, AKT3, as shown in Fig.4.10(a), Fig.4.10(b), and Fig.4.10(c), respectively. The

gene expression levels were up-regulated by 1.35 to 1.44-fold compared with the 2% FBS control group. Meanwhile, there was no significant difference on gene expression between the LAMS group and the 2% FBS control group. Nevertheless, the Enos expression (Fig.4.10(d)) in the LAMS group was slightly higher than that of the control group. The eNOs expression of the G-LAMS group was 1.75-fold higher than that of the control group. The results indicated that the vascularization of G-LAMS to HUVECs was to go through the pathway of PI3K, Akt, and eNOS from upstream to downstream gene expression.

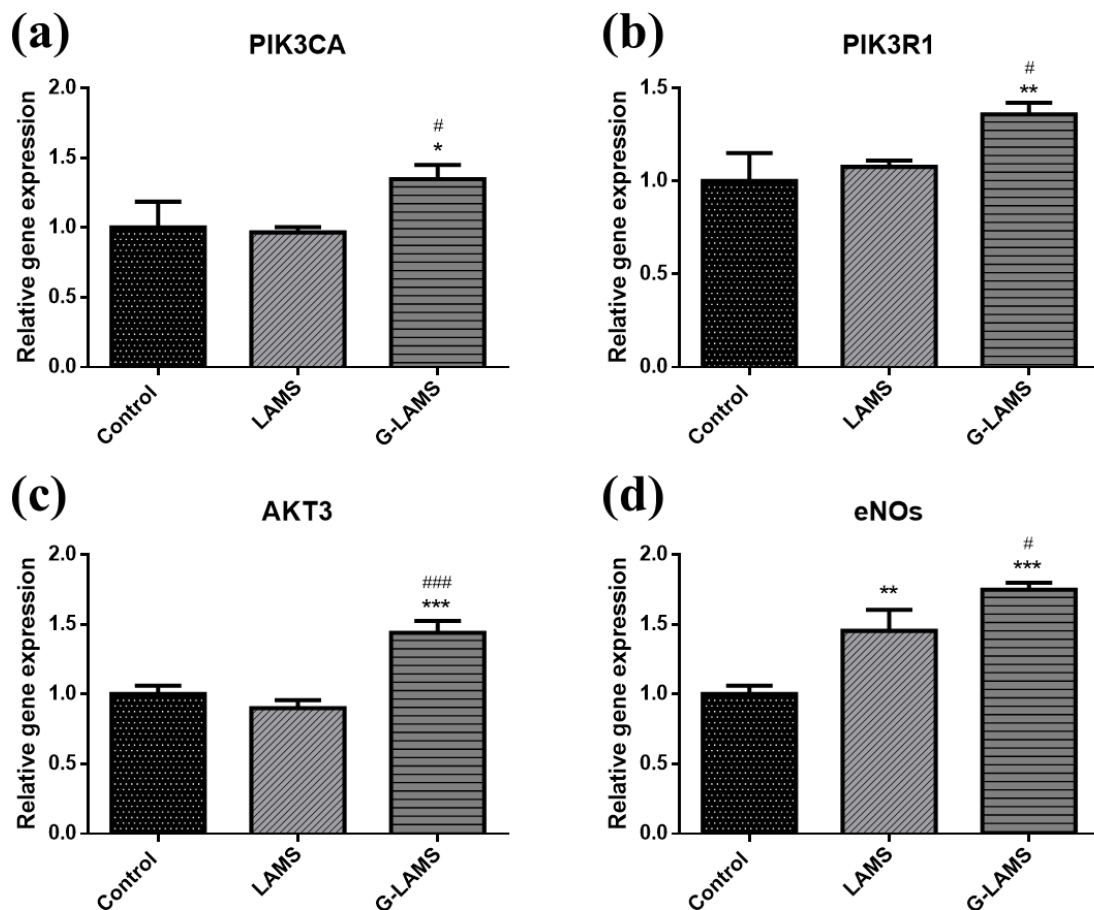


**Fig.4.10** Gene expression of HUVECs after starvation for 4 hours and then treated with materials for 1 hour. Relative (a) PIK3CA (b) PIK3R1 (c) AKT3 (d) eNOs gene expression was measured by Q-PCR and normalized by GAPDH gene expression. (n = 3) ( $p < 0.05$ , \*;  $p < 0.01$ , \*\*;  $p < 0.001$ , \*\*\* compared to control group;  $p < 0.05$ , #;  $p < 0.01$ ,

##;  $p < 0.001$ , ### compared to LAMS group by one-way ANOVA with Tukey's multiple comparisons test.)



#### 4.9 Evaluation of G-LAMS on genotoxicity chromosome aberration assay

CHO cells were used to evaluate G-LAMS on genotoxicity; where the control group was in blank medium and the experimental group was the extract of G-LAMS (Fig.4.11). A total of 70 well spread chromosomes could be examined under the DIC microscope by Giemsa stain. Fisher's exact test was used to analyze the statistical data. There was no significant difference in the chromosome aberration between the control group and experimental group, which was summarized in Table 4.1.

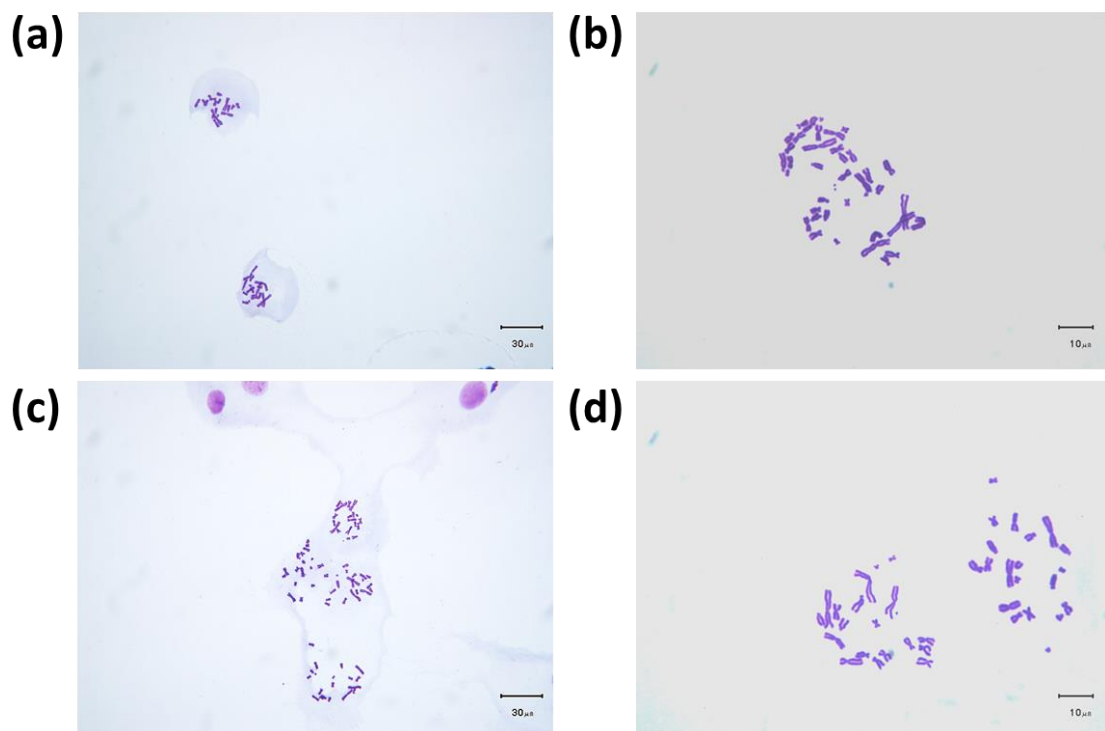


**Fig.4.11** The evaluation of the genotoxicity assay was determined by CHO cells chromosome aberration assay. CHO cells were treated by (a) negative control observed under 40X magnification and (b) negative control examined under 100X magnification; the aberrations would be compared with (c) experimental group added with G-LAMS extract observed under 40X magnification and (d) experimental group added with G-



LAMS extract observed under 100X magnification.

**Table 4.1** The chromosome aberration data of the negative control group and the G-LAMS treated CHO cells \*.

Treatment	Aberrant metaphases	Total metaphases	Aberration frequency	P-value
Control	5	70	0.071	
G-LAMS	2	70	0.029	NS

\* A summary data of the genotoxicity results from the negative control group and G-LAMS treated CHO cells. P-value derived from Fisher's exact test. NS = Not significant.

#### 4.10 Histological and Immunofluorescence Analysis

Fig.4.12, (Fig.4.13(a)) (Fig.4.13(b)). (Fig.4.13). Fig.4.13(a) Fig.4.14 and Fig.4.15.

The adipogenic differentiation of isolated ADSCs was assessed using Oil Red O staining, which indicated successful differentiation into adipocytes upon signal induction.

The corresponding figures, labeled as Fig.4.12. display the results of the staining.

To evaluate the adipogenesis of ADSC-G-LAMS encapsulated with adipocytes (ADSC-G-LAMS-adipocyte), CD31 immuno-staining and H&E staining were performed at the 4th week after subcutaneous injection. Confocal microscopy images (Fig.4.13(a)) displayed the nuclei stained with DAPI, ADSCs labeled in blue and green due to GFP expression, and CD31, a major marker of endothelial cells, depicted in red. The angiogenesis quantification was determined by calculating the relative cell number in the CD31 fluorescence image using ImageJ software (Fig.4.13(b)). The ADSC-LAMS-adipocyte group and ADSC-G-LAMS-adipocyte group exhibited significantly higher

numbers of endothelial cells compared to the ADSC-adipocyte group. Notably, the microspheres containing Rg1 (ADSC-G-LAMS-adipocyte) displayed the highest number of endothelial cells in adipose tissue, surpassing the microspheres without Rg1 (ADSC-LAMS-adipocyte) (Fig.4.13). The H&E staining corroborated these findings, showing an increased number of neo-blood vessels (indicated by an arrow in (a)) in the ADSC-G-LAMS-adipocyte group compared to the other two groups. Additionally, the injected microspheres (indicated by an asterisk) were fully integrated with the host tissue. Furthermore, the graft volume of the materials was evaluated and quantified after sacrificing the animals, as illustrated in Fig.4.14 and Fig.4.15.

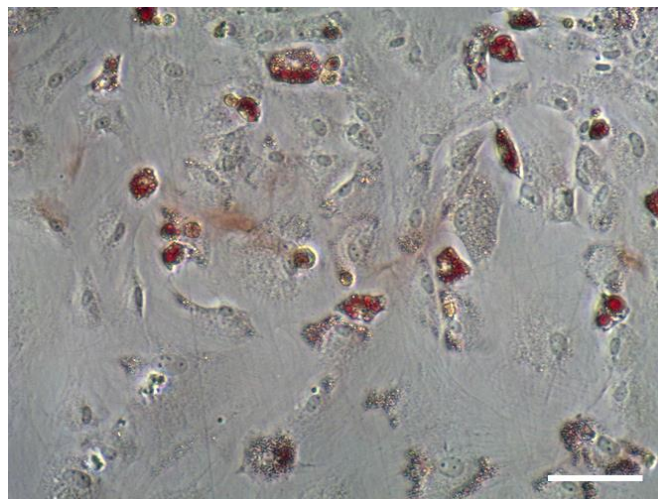


**Fig.4.12** Oil Red O staining image of the adipogenic differentiation induced ADSCs.

Scale bar = 20  $\mu$ m.

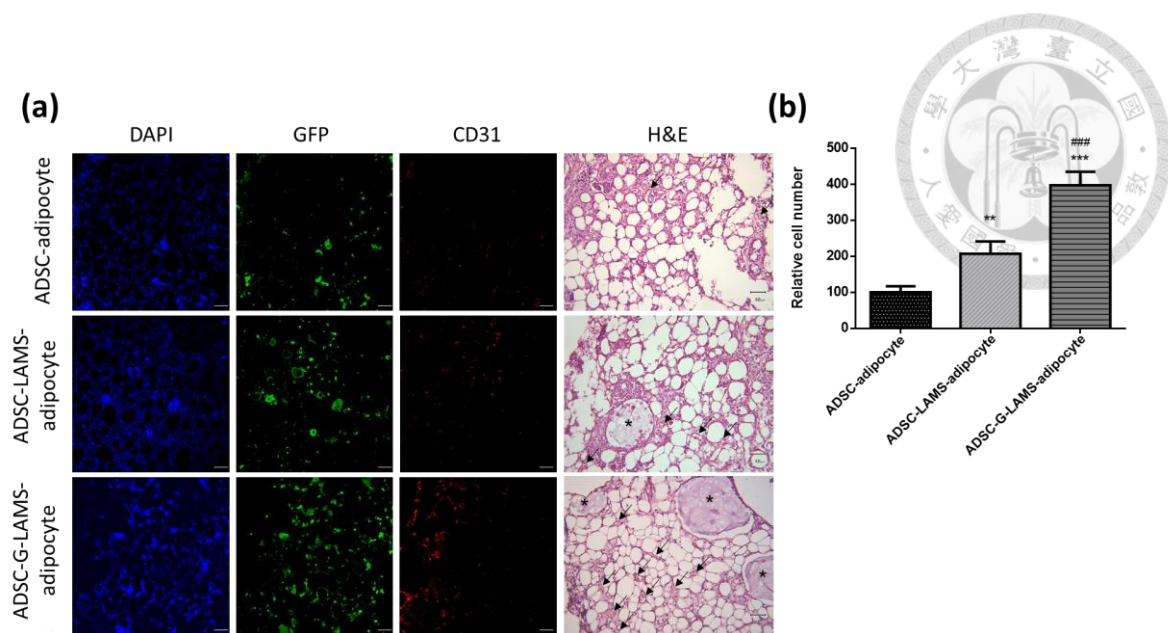


**Fig.4.13** *In vivo* analysis of grafts after 4 weeks (a) Immunofluorescence staining of CD31 on adipose tissue sections from the implant site. CD31 was used as an endothelial cell marker. Nuclei were stained with DAPI, and GFP-positive cells were observed by confocal microscopy. In H&E staining, arrows indicate blood vessels, and asterisks indicate the implanted microspheres. Scale bar = 100  $\mu$ m, (b) Quantification of angiogenesis was determined by calculating relative cell number in CD31 fluorescence image by ImageJ. (Data in (b) were measured by four independent experiments, and at least five fields were taken per section.) ( $p < 0.05$ , \*;  $p < 0.01$ , \*\*;  $p < 0.001$ , \*\*\*, compared to the ADSC–adipocyte group;  $p < 0.05$ , #;  $p < 0.01$ , ##;  $p < 0.001$ , ### compared to the ADSC–LAMS–adipocyte group by one-way ANOVA with Tukey's multiple comparisons test.).



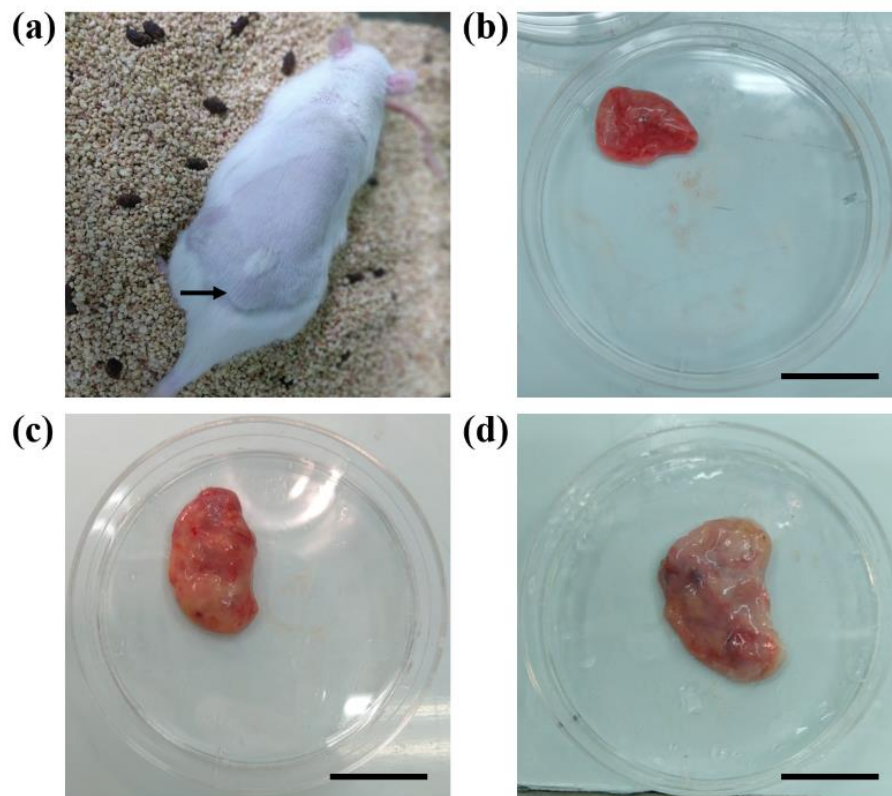


**Fig.4.14** The pictures of implanted materials after 4 weeks of transplantation. (a) Represented picture of the rats (ADSC-G-LAMS-adipocyte group) *in vivo* study. The black arrow indicated the implanted materials. (b) ADSC-adipocyte group. (c) ADSC-LAMS-adipocyte group. (d) ADSC-G-LAMS-adipocyte group. Scale bar = 1 cm.

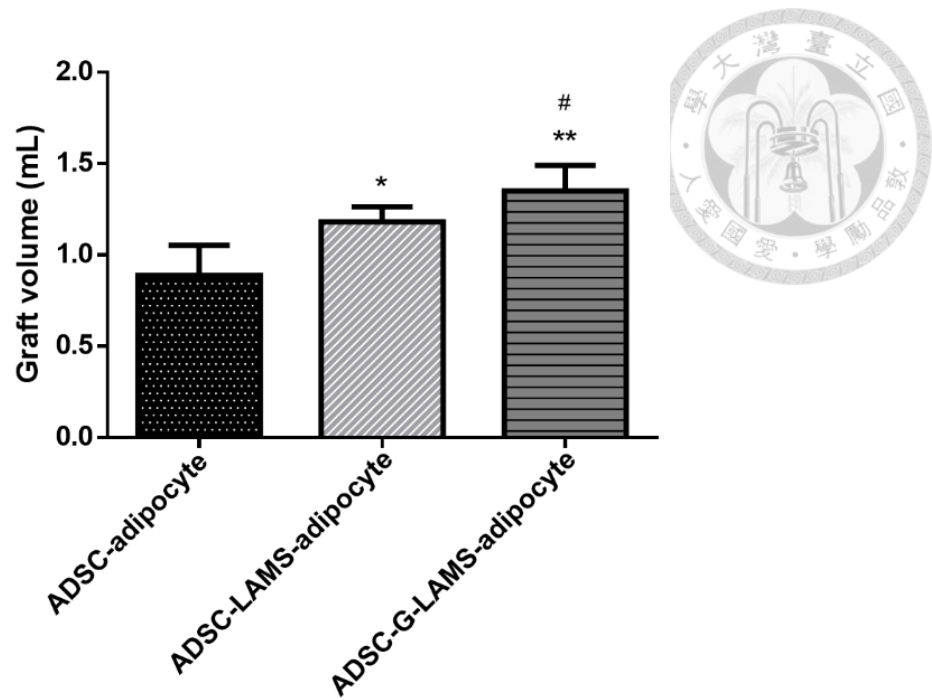


**Fig.4.15** The graft volume of implanted materials after 4 weeks of transplantation. ( $p < 0.05$ , \*;  $p < 0.01$ , \*\*, compared to the ADSC–adipocyte group;  $p < 0.05$ , #, compared to ADSC–LAMS–adipocyte group.)

#### 4.11 Blood element analysis and serological analysis

The whole blood was collected from rats, before being sacrificed, for blood element and serological analysis. Compared with the reference value (Charles River Laboratories, CD® IGS Rat Model Information Sheet), the data in blood element analysis (Table 4.2) and serological analysis (Table 4.3) were all in the normal range. The results could tell that the laminin-alginate microspheres no matter with or without Rg1 all showed no systemic toxicity.

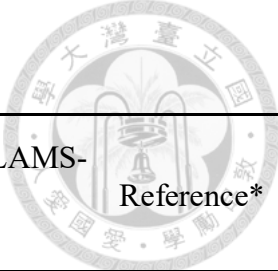


**Table 4.2** Summary of blood element analysis.

	ADSC-Adipocyte	ADSC-LAMS- Adipocyte	ADSC-G-LAMS- Adipocyte	Reference*
RBC (M/ $\mu$ L)	8.27 $\pm$ 0.41	7.67 $\pm$ 0.36	8.03 $\pm$ 0.42	7.37 $\pm$ 1.09
HGB (g/dL)	16.90 $\pm$ 0.62	15.20 $\pm$ 0.89	15.57 $\pm$ 1.03	16.52 $\pm$ 2.72
HCT (%)	52.57 $\pm$ 3.33	44.12 $\pm$ 4.20	47.17 $\pm$ 2.84	48.45 $\pm$ 7.14
MCV (fL)	63.57 $\pm$ 1.60	60.16 $\pm$ 1.23	58.77 $\pm$ 0.83	65.49 $\pm$ 6.46
MCH (pg)	20.47 $\pm$ 0.80	19.80 $\pm$ 0.35	19.37 $\pm$ 0.34	22.40 $\pm$ 1.35
MCHC (g/dL)	32.20 $\pm$ 1.04	32.94 $\pm$ 0.26	33.00 $\pm$ 0.22	34.10 $\pm$ 2.34
PLT(K/ $\mu$ L)	1274.67 $\pm$ 339.01	1109.80 $\pm$ 170.04	1182.67 $\pm$ 21.14	1583.22 $\pm$ 378.23
WBC (K/ $\mu$ L)	9.09 $\pm$ 0.62	9.10 $\pm$ 2.59	9.03 $\pm$ 1.90	10.17 $\pm$ 3.72
NEUT (K/ $\mu$ L)	2.72 $\pm$ 0.85	2.43 $\pm$ 1.75	3.25 $\pm$ 2.03	2.62 $\pm$ 1.24
LYMPH (K/ $\mu$ L)	5.49 $\pm$ 1.10	6.24 $\pm$ 2.35	5.18 $\pm$ 0.23	6.73 $\pm$ 2.64
MONO (K/ $\mu$ L)	0.72 $\pm$ 0.43	0.25 $\pm$ 0.07	0.41 $\pm$ 0.10	0.62 $\pm$ 0.28
EO (K/ $\mu$ L)	0.14 $\pm$ 0.05	0.16 $\pm$ 0.04	0.16 $\pm$ 0.05	0.15 $\pm$ 0.16
BASO (K/ $\mu$ L)	0.02 $\pm$ 0.01	0.02 $\pm$ 0.02	0.04 $\pm$ 0.01	0.04 $\pm$ 0.05

\* Charles River Laboratories, CD® IGS Rat Model Information Sheet. RBC: red blood cell; HGB: hemoglobin; HCT: hematocrit; MCV: mean corpuscular volume; MCH: mean corpuscular hemoglobin; MCHC: mean corpuscular hemoglobin concentration; PLT: platelet; WBC: white blood cell; NEUT: neutrophil; LYMPH: lymphocyte; MONO: monocyte; EO: eosinophil; BASO: basophil.

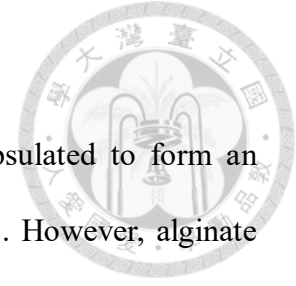
**Table 4.3** Summary of serological analysis.



	ADSC-Adipocyte	ADSC-LAMS- Adipocyte	ADSC-G-LAMS- Adipocyte	Reference*
ALT (U/L)	46.25 ± 5.54	40.80 ± 2.56	48.25 ± 13.37	56.72 ± 32.40
AST (U/L)	82.40 ± 6.06	82.12 ± 6.64	114.45 ± 54.42	111.88 ± 65.11
BUN (mg/dL)	17.92 ± 2.84	16.25 ± 1.71	16.73 ± 1.93	13.45 ± 4.19
Crea (mg/dL)	0.45 ± 0.11	0.50 ± 0.15	0.43 ± 0.04	0.47 ± 0.10

\* Charles River Laboratories, CD® IGS Rat Model Information Sheet. ALT: alanine aminotransferase; AST: aspartate aminotransferase; BUN: blood urea nitrogen; Crea: creatinine.

## Chapter 5 DISCUSSION



Alginate is a biodegradable polymer that cells can be encapsulated to form an injectable hydrogel, beads, and the preformed scaffolds [4, 38, 39]. However, alginate lacks domains for cell recognition. Laminin, one of the major extracellular matrix glycoproteins, was reported to play an important role to influence cell differentiation, migration, and adhesion in the early embryonic stage [41-43].

In the study, laminin was modified to alginate by a relatively low concentration of sodium periodate ( $\text{NaIO}_4$ ) with a long reaction time to synthesize laminin-modified alginate for better cell viability and lower cytotoxicity as shown in Fig.4.6 and Fig.4.7. The developed laminin-modified alginate was mixed with ADSCs and Rg1 in the medium; thereafter, sprayed into a calcium chloride ( $\text{CaCl}_2$ ) solution to prepare microsphere (abbreviated as ADSC-G-LAMS) by bio-electrospray with a power syringe. The prepared ADSC-G-LAMS microspheres were collected and combined with adipocytes to produce necessary growth factors to make ADSCs toward the adipogenic pathway.

It has been reported that the diameter of the microsphere should be smaller than 350  $\mu\text{m}$  to minimize fibrosis reaction [79]. The fibrosis reaction will cause fibrous capsule contraction and result in the implanted breast having a poor tactile quality [80]. In addition to this, one of the most challenging issues for 3D scaffolds in tissue engineering is the need for adequate and rapid vascularization, as the diffusion of nutrients and oxygen can only occur over 200-300 microns [81]. Therefore, the size control of biomaterial scaffold is very important. The average diameter of the microspheres prepared by using the bio-electrospray methods was  $232.42 \pm 42.37 \mu\text{m}$  (Fig.4.5); that was more convenient for injection. In addition, the smaller diameter could shorten the diffusion distance of the

nutrition and oxygen to make an encapsulated cell in high proliferation and survival rate (Fig.4.5, Fig.4.6 and Fig.4.7).

Ginsenoside, Rg1 has estrogen-like properties that can interact with the glucocorticoid receptor and activation of the nitric oxide synthase [55, 56]. Nitric oxide is well known to be an important factor in the mediation of angiogenesis and proliferation of endothelial cells [55, 58]. It was noted that the bioactivity of Rg1 is not affected by temperature, pH, and solvents compared to protein-based growth factors [60]. Rg1 also could affect MSCs proliferation, differentiation, apoptosis [82]. One of the studies showed that Rg1 could promote human BMSCs toward endothelial differentiation *in vitro* [83]. Other results also showed that Rg1 could attract BMSCs to migrate to local myocardial tissues and differentiate into vascular endothelial cells for capillary regeneration of infarcted myocardium tissue *in vivo* [84]. Besides, it was reported that Rg1 had been mixed with the collagen and increased the micro-vessel density in the nude mice model for soft tissue regeneration [85]. In this study, Rg1 was selected as a bioactive molecule, enclosed in the laminin-modified alginate microspheres, and proved tube formation by Matrigel™ model (Fig.4.8 and Fig.4.9). In the study of the Rg1 releasing profile, an initial burst happened on the first day. We believe that was needed to give enough signals to attract the MSCs for tissue reconstruction (Fig.4.8). The sustained release of the Rg1 was to induce encapsulated ADSCs or homing MSCs toward neo-vascularization to keep injected ADSCs or adipocytes survive to join the tissue growth and repair.

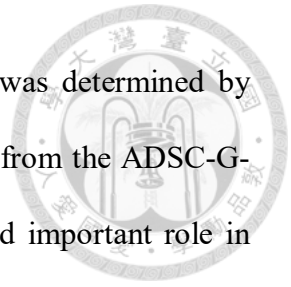
In the study, several genes were selected to confirm that the PI3K/AKT was the major pathway to induce HUVEC vascularization under Rg1 stimulation (Fig.4.10(a), Fig.4.10(b) and Fig.4.10(c)). The genes related to PI3K/AKT pathway were all up-

regulated in HUVECs cultured with the G-LAMS. In addition, the gene expression of eNOs was up-regulated as well (Fig.4.10(d)).

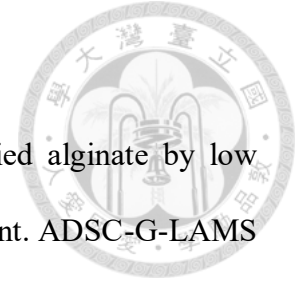
We noticed that eNOs gene expression in LAMS was much higher than that of the control group, however, there was no significant difference in the gene expression related to the PI3K/AKT pathway. It had shown that laminin could influence endothelial shear sensing and mechano-transduction through the focal adhesion kinase (FAK). The shear-induced eNOs synthesis may happen in endothelial cells [86-88]. We believe that the difference of eNOs expression between the LAMS group and control group might be partially attributed to laminin rather than Rg1. The detailed mechanism of laminin action is not much discussed in this research, but it still provides us with promising results, that the combination of Rg1 with laminin modified alginate carrier can have significant impacts on angiogenic properties. The results of chromosome aberration by CHO cells and Giemsa stain showed that the synthesized G-LAMS was no concern to genotoxicity as shown in Fig.4.11 and summarized in Table 4.1.

In adipose tissue engineering, new blood vessel formation is important for transplanted cell survival and reduces grafting volume shrinkage [89]. In animal studies, the materials were co-cultured with autologous adipose tissue, becoming an injectable engineered fat. The adipocyte was reported to release various signals to regulate local MSCs or ADSCs toward adipogenic differentiation [62-65]. The results of the animal study showed that the group of ADSC-G-LAMS-adipocyte exhibited the highest number of neo-blood vessel and endothelial cells with obvious adipogenesis as shown in Fig.4.13. The results of the blood element analysis and serological analysis were to further confirm the safety of the prepared cell-laden adipose graft (Table 4.2 and Table 4.3).

In this study, the efficacy of the developed ADSC-G-LAMS was determined by comparing it with ADSC-LAMS and ADSC. The Rg1 released out from the ADSC-G-LAMS was to enhance angiogenesis. ADSCs and adipocytes played important role in adipogenesis. Those were proved both *in vitro* and *in vivo*. In the future, the microspheres prepared in this study might be developed to deliver other bioactive molecules, growth factors, and drugs for other applications in stem cell therapy and tissue engineering.

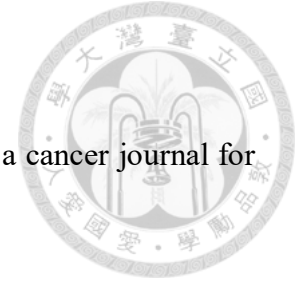


## Chapter 6 CONCLUSION



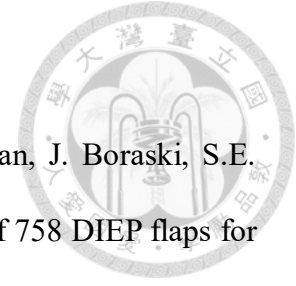
In the study, we successfully synthesized the laminin-modified alginate by low concentration sodium periodate to mimic the embryonic environment. ADSC-G-LAMS were prepared by bio-electrospray methods. The average diameter of the microspheres prepared by using the bio-electrospray methods was  $232.42 \pm 42.37 \mu\text{m}$ ; that was more convenient for injection. The developed ADSC-G-LAMS microspheres could provide a good environment to allow ADSCs to survive, proliferate, and toward desired differentiation pathway without cytotoxicity, genotoxicity, and systemic toxicity. The released Rg1 can induce HUVEC cells vascularization property to enhance 35.9% of total tube lengths to that of the control group. The mechanism of the vascularization of G-LAMS to HUVECs was to go through the pathway of PI3K, Akt, and eNOS from upstream to downstream gene expression. There were two stages of Rg1 release from the microspheres with an initial burst release of 67%; that was believed to give enough signals to attract the MSCs for tissue reconstruction. After that, the sustained release of the Rg1 could induce encapsulated ADSCs or homing MSCs toward neo-vascularization to enhance ADSCs or adipocytes survival rate to join the tissue growth and repair with adipogenesis for breast reconstruction after lumpectomy. The results of the animal study showed that ADSC-G-LAMS microspheres could integrate well into the host adipose tissue with an adequate rate of angiogenesis by constantly releasing Rg1 for breast reconstruction. The group of ADSC-G-LAMS-adipocyte group exhibited the 1.52-fold graft volume to the ADSC-adipocyte group and had the highest number of neo-blood vessel and endothelial cells with obvious adipogenesis. These findings fully support that the ADSC-G-LAMS could be the potential scaffolds for stem cell and angiogenic factor carriers for adipose tissue engineering.

## Chapter 7 REFERENCE



- [1] R.L. Siegel, K.D. Miller, A. Jemal, Cancer statistics, 2019, CA: a cancer journal for clinicians 69(1) (2019) 7-34.
- [2] A.C. Society, Breast cancer facts & figures 2019–2020, Am. Cancer Soc (2019) 1-44.
- [3] F.-C. Liu, H.-T. Lin, C.-F. Kuo, L.-C. See, M.-J. Chiou, H.-P. Yu, Epidemiology and survival outcome of breast cancer in a nationwide study, Oncotarget 8(10) (2017) 16939.
- [4] K.J. Burg, B. Inskeep, T.C. Burg, Breast Tissue Engineering: Reconstruction Implants and Three-Dimensional Tissue Test Systems, Principles of Tissue Engineering, Elsevier 2014, pp. 727-749.
- [5] T. Cronin, F. Gerow, Augmentation Mammoplasty: A New "Natural Feel" Prosthesis, read before the Third International Congress of Plastic Surgery, Washington, DC, 1963.
- [6] T.D. Cronin, Augmentation mammoplasty: a new "natural feel" prosthesis, Transact, III Internat Congr Plast Surg (1964).
- [7] E.J. Giltay, H.B. Moens, A.H. Riley, R.G. Tan, Silicone breast prostheses and rheumatic symptoms: a retrospective follow up study, Annals of the rheumatic diseases 53(3) (1994) 194-196.
- [8] R. Gayou, R. Rudolph, Capsular contraction around silicone mammary prostheses, Annals of plastic surgery 2(1) (1979) 62-71.
- [9] H. Holmström, The free abdominoplasty flap and its use in breast reconstruction: An experimental study and clinical case report, Scandinavian journal of plastic and reconstructive surgery 13(3) (1979) 423-427.
- [10] J.C. Selber, J.E. Kurichi, S.J. Vega, S.S. Sonnad, J.M. Serletti, Risk factors and complications in free TRAM flap breast reconstruction, Annals of plastic surgery 56(5)





(2006) 492-497.

[11] P.S. Gill, J.P. Hunt, A.B. Guerra, F.J. Dellacroce, S.K. Sullivan, J. Boraski, S.E. Metzinger, C.L. Dupin, R.J. Allen, A 10-year retrospective review of 758 DIEP flaps for breast reconstruction, *Plastic and reconstructive surgery* 113(4) (2004) 1153-1160.

[12] I. Van Nieuwenhove, L. Tytgat, M. Ryx, P. Blondeel, F. Stillaert, H. Thienpont, H. Ottevaere, P. Dubruel, S. Van Vlierberghe, Soft tissue fillers for adipose tissue regeneration: From hydrogel development toward clinical applications, *Acta biomaterialia* 63 (2017) 37-49.

[13] M.J. McCleave, Is breast augmentation using hyaluronic acid safe?, *Aesthetic plastic surgery* 34(1) (2010) 65-68.

[14] U.S.F.a.D. Administration, FDA-Approved Dermal Fillers, 2020.

[15] J.P. Vacanti, A. Atala, D.J. Mooney, R.S. Langer, Breast tissue engineering, *Google Patents*, 1998.

[16] G. Ailhaud, E. Amri, C. Cermolacce, P. Djian, C. Forest, D. Gaillard, P. Grimaldi, J. Khoo, R. Negrel, G. Serrero-Davé, Hormonal requirements for growth and differentiation of ob17 preadipocyte cells in vitro, *Diabete & metabolisme* 9(2) (1983) 125-133.

[17] H. Green, M. Meuth, An established pre-adipose cell line and its differentiation in culture, *Cell* 3(2) (1974) 127-133.

[18] J.H. Choi, J.M. Gimble, K. Lee, K.G. Marra, J.P. Rubin, J.J. Yoo, G. Vunjak-Novakovic, D.L. Kaplan, Adipose tissue engineering for soft tissue regeneration, *Tissue Engineering Part B: Reviews* 16(4) (2010) 413-426.

[19] J.M. Gimble, A.J. Katz, B.A. Bunnell, Adipose-derived stem cells for regenerative medicine, *Circulation research* 100(9) (2007) 1249-1260.

[20] I. Van Nieuwenhove, L. Tytgat, M. Ryx, P. Blondeel, F. Stillaert, H. Thienpont, H.

Ottevaere, P. Dubruel, S.J.A.b. Van Vlierberghe, Soft tissue fillers for adipose tissue regeneration: From hydrogel development toward clinical applications, 63 (2017) 37-49.

[21] J.R. Mauney, T. Nguyen, K. Gillen, C. Kirker-Head, J.M. Gimble, D.L. Kaplan, Engineering adipose-like tissue in vitro and in vivo utilizing human bone marrow and adipose-derived mesenchymal stem cells with silk fibroin 3D scaffolds, *Biomaterials* 28(35) (2007) 5280-5290.

[22] S.-W. Kang, S.-W. Seo, C.Y. Choi, B.-S. Kim, Porous poly (lactic-co-glycolic acid) microsphere as cell culture substrate and cell transplantation vehicle for adipose tissue engineering, *Tissue Engineering Part C: Methods* 14(1) (2008) 25-34.

[23] S.-D. Lin, K.-H. Wang, A.-P. Kao, Engineered adipose tissue of predefined shape and dimensions from human adipose-derived mesenchymal stem cells, *Tissue Engineering Part A* 14(5) (2008) 571-581.

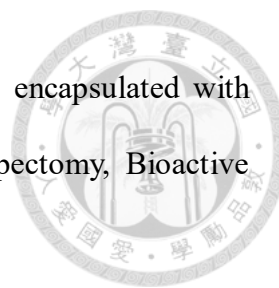
[24] R.M. Shanti, S. Janjanin, W.-J. Li, L.J. Nesti, M.B. Mueller, M.B. Tzeng, R.S. Tuan, In vitro adipose tissue engineering using an electrospun nanofibrous scaffold, *Annals of plastic surgery* 61(5) (2008) 566-571.

[25] B. Weiser, L. Prantl, T.E. Schubert, J. Zellner, C. Fischbach-Teschl, T. Spruss, A.K. Seitz, J. Tessmar, A. Goepferich, T. Blunk, In vivo development and long-term survival of engineered adipose tissue depend on in vitro precultivation strategy, *Tissue Engineering Part A* 14(2) (2008) 275-284.

[26] P.A. Gunatillake, R. Adhikari, Biodegradable synthetic polymers for tissue engineering, *Eur Cell Mater* 5(1) (2003) 1-16.

[27] I. Rajzer, E. Menaszek, O. Castano, Electrospun polymer scaffolds modified with drugs for tissue engineering, *Materials Science and Engineering: C* 77 (2017) 493-499.

[28] I.-H. Yang, Y.-S. Chen, J.-J. Li, Y.-J. Liang, T.-C. Lin, S. Jakfar, M. Thacker, S.-C.



Wu, F.-H. Lin, The development of laminin-alginate microspheres encapsulated with Ginsenoside Rg1 and ADSCs for breast reconstruction after lumpectomy, *Bioactive Materials* 6(6) (2021) 1699-1710.

[29] D. Von Heimburg, M. Kuberka, R. Rendchen, K. Hemmrich, G. Rau, N. Pallua, Preadipocyte-loaded collagen scaffolds with enlarged pore size for improved soft tissue engineering, *The International journal of artificial organs* 26(12) (2003) 1064-1076.

[30] K. Hemmrich, D. von Heimburg, R. Rendchen, C. Di Bartolo, E. Milella, N. Pallua, Implantation of preadipocyte-loaded hyaluronic acid-based scaffolds into nude mice to evaluate potential for soft tissue engineering, *Biomaterials* 26(34) (2005) 7025-7037.

[31] Y. Kimura, M. Ozeki, T. Inamoto, Y. Tabata, Adipose tissue engineering based on human preadipocytes combined with gelatin microspheres containing basic fibroblast growth factor, *Biomaterials* 24(14) (2003) 2513-2521.

[32] W.S. Kim, D.J. Mooney, P.R. Arany, K. Lee, N. Huebsch, J. Kim, Adipose tissue engineering using injectable, oxidized alginate hydrogels, *Tissue Engineering Part A* 18(7-8) (2012) 737-743.

[33] H. Hauner, P. Schmid, E.-F. Pfeiffer, Glucocorticoids and insulin promote the differentiation of human adipocyte precursor cells into fat cells, *The Journal of Clinical Endocrinology & Metabolism* 64(4) (1987) 832-835.

[34] O. Wiederer, G. Löffler, Hormonal regulation of the differentiation of rat adipocyte precursor cells in primary culture, *Journal of lipid research* 28(6) (1987) 649-658.

[35] C. Pantoja, J.T. Huff, K.R. Yamamoto, Glucocorticoid signaling defines a novel commitment state during adipogenesis in vitro, *Molecular biology of the cell* 19(10) (2008) 4032-4041.

[36] H. Hauner, G. Entenmann, M. Wabitsch, D. Gaillard, G. Ailhaud, R. Negrel, E.-F.



Pfeiffer, Promoting effect of glucocorticoids on the differentiation of human adipocyte precursor cells cultured in a chemically defined medium, *The Journal of clinical investigation* 84(5) (1989) 1663-1670.

[37] S. Niemelä, S. Miettinen, J. Sarkanen, N. Ashammakhi, Adipose tissue and adipocyte differentiation: molecular and cellular aspects and tissue engineering applications, *Topics in Tissue Engineering* 4(1) (2008) 26.

[38] C. Halberstadt, C. Austin, J. Rowley, C. Culberson, A. Loeb sack, S. Wyatt, S. Coleman, L. Blacksten, K. Burg, D.J.T.e. Mooney, A hydrogel material for plastic and reconstructive applications injected into the subcutaneous space of a sheep, 8(2) (2002) 309-319.

[39] K.Y. Lee, D.J. Mooney, Alginate: properties and biomedical applications, *Progress in polymer science* 37(1) (2012) 106-126.

[40] N. Shaari, S.K. Kamarudin, Recent advances in additive-enhanced polymer electrolyte membrane properties in fuel cell applications: An overview, *International Journal of Energy Research* 43(7) (2019) 2756-2794.

[41] I. Leivo, A. Vaheri, R. Timpl, J. Wartiovaara, Appearance and distribution of collagens and laminin in the early mouse embryo, *Developmental biology* 76(1) (1980) 100-114.

[42] E. Hohenester, P.D. Yurchenco, Laminins in basement membrane assembly, *Cell adhesion & migration* 7(1) (2013) 56-63.

[43] S. Li, D. Edgar, R. Fässler, W. Wadsworth, P.D. Yurchenco, The role of laminin in embryonic cell polarization and tissue organization, *Developmental cell* 4(5) (2003) 613-624.

[44] S.S. Rao, J. Winter, Adhesion molecule-modified biomaterials for neural tissue



engineering, *Frontiers in neuroengineering* 2 (2009) 6.

[45] Y.-S. Hsueh, Y.-S. Chen, H.-C. Tai, O. Mestak, S.-C. Chao, Y.-Y. Chen, Y. Shih, J.-F. Lin, M.-J. Shieh, F.-H. Lin, Laminin-alginate beads as preadipocyte carriers to enhance adipogenesis in vitro and in vivo, *Tissue Engineering Part A* 23(5-6) (2017) 185-194.

[46] Y.S. Chen, Y.Y. Chen, Y.S. Hsueh, H.C. Tai, F.H. Lin, Modifying alginate with early embryonic extracellular matrix, laminin, and hyaluronic acid for adipose tissue engineering, *Journal of Biomedical Materials Research Part A* 104(3) (2016) 669-677.

[47] G. Hermanson, The reactions of bioconjugation, *Bioconjugate techniques* 3 (2013) 229-258.

[48] Y.-C. Chen, W.-Y. Su, S.-H. Yang, A. Gefen, F.-H. Lin, In situ forming hydrogels composed of oxidized high molecular weight hyaluronic acid and gelatin for nucleus pulposus regeneration, *Acta biomaterialia* 9(2) (2013) 5181-5193.

[49] W.-Y. Su, Y.-C. Chen, F.-H. Lin, Injectable oxidized hyaluronic acid/adipic acid dihydrazide hydrogel for nucleus pulposus regeneration, *Acta biomaterialia* 6(8) (2010) 3044-3055.

[50] S.Y. Sheu, W.S. Chen, J.S. Sun, F.H. Lin, T. Wu, Biological characterization of oxidized hyaluronic acid/resveratrol hydrogel for cartilage tissue engineering, *Journal of Biomedical Materials Research Part A: An Official Journal of The Society for Biomaterials, The Japanese Society for Biomaterials, and The Australian Society for Biomaterials and the Korean Society for Biomaterials* 101(12) (2013) 3457-3466.

[51] G. Sitterley, S. Karmiöl, E. Manaster, J. Ryn, Attachment and matrix factors, *Biofiles (Sigma-Aldrich)* 3 (2008) 1-28.

[52] M. Lovett, K. Lee, A. Edwards, D.L. Kaplan, Vascularization strategies for tissue engineering, *Tissue Engineering Part B: Reviews* 15(3) (2009) 353-370.

[53] C.D. Ley, M.W. Olsen, E.L. Lund, P.E. Kristjansen, Angiogenic synergy of bFGF and VEGF is antagonized by Angiopoietin-2 in a modified in vivo Matrigel assay, *Microvascular research* 68(3) (2004) 161-168.

[54] D.F. Lazarous, M. Scheinowitz, M. Shou, E. Hodge, M.S. Rajanayagam, S. Hunsberger, W.G. Robison Jr, J.A. Stiber, R. Correa, S.E. Epstein, Effects of chronic systemic administration of basic fibroblast growth factor on collateral development in the canine heart, *Circulation* 91(1) (1995) 145-153.

[55] R.Y. Chan, W.-F. Chen, A. Dong, D. Guo, M.-S. Wong, Estrogen-like activity of ginsenoside Rg1 derived from *Panax notoginseng*, *The Journal of Clinical Endocrinology & Metabolism* 87(8) (2002) 3691-3695.

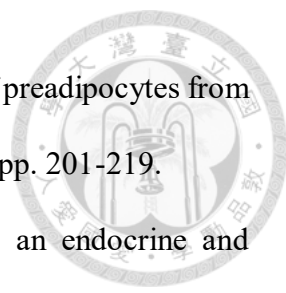
[56] L.W. Cheung, K.W. Leung, C.K. Wong, R.N. Wong, A.S. Wong, Ginsenoside-Rg1 induces angiogenesis via non-genomic crosstalk of glucocorticoid receptor and fibroblast growth factor receptor-1, *Cardiovascular research* 89(2) (2011) 419-425.

[57] P.Y.K. Yue, N.K. Mak, Y.K. Cheng, K.W. Leung, T.B. Ng, D.T.P. Fan, H.W. Yeung, R.N.S. Wong, Pharmacogenomics and the Yin/Yang actions of ginseng: anti-tumor, angiomodulating and steroid-like activities of ginsenosides, *Chinese medicine* 2(1) (2007) 6.

[58] J.P. Cooke, D.W. Losordo, Nitric oxide and angiogenesis, *Am Heart Assoc*, 2002.

[59] S. Sengupta, S.-A. Toh, L.A. Sellers, J.N. Skepper, P. Koolwijk, H.W. Leung, H.-W. Yeung, R.N. Wong, R. Sasisekharan, T.-P.D. Fan, Modulating angiogenesis: the yin and the yang in ginseng, *Circulation* 110(10) (2004) 1219-1225.

[60] L.-C. Yu, S.-C. Chen, W.-C. Chang, Y.-C. Huang, K.M. Lin, P.-H. Lai, H.-W. Sung, Stability of angiogenic agents, ginsenoside Rg1 and Re, isolated from *Panax ginseng*: in vitro and in vivo studies, *International journal of pharmaceutics* 328(2) (2007) 168-176.

- 
- [61] D.B. Hausman, H.J. Park, G.J. Hausman, Isolation and culture of preadipocytes from rodent white adipose tissue, *Adipose tissue protocols*, Springer2008, pp. 201-219.
- [62] V. Mohamed-Ali, J. Pinkney, S. Coppack, Adipose tissue as an endocrine and paracrine organ, *International journal of obesity* 22(12) (1998) 1145.
- [63] Y. Deng, P.E. Scherer, Adipokines as novel biomarkers and regulators of the metabolic syndrome, *Annals of the New York Academy of Sciences* 1212 (2010) E1.
- [64] F. Stillaert, M. Findlay, J. Palmer, R. Idrizi, S. Cheang, A. Messina, K. Abberton, W. Morrison, E.W. Thompson, Host rather than graft origin of Matrigel-induced adipose tissue in the murine tissue-engineering chamber, *Tissue engineering* 13(9) (2007) 2291-2300.
- [65] L. Wu, T. Wang, Y. Ge, X. Cai, J. Wang, Y. Lin, Secreted factors from adipose tissue increase adipogenic differentiation of mesenchymal stem cells, *Cell proliferation* 45(4) (2012) 311-319.
- [66] L.T. Nguyen, A.O. Odeleye, C.Y. Chui, T. Baudequin, Z. Cui, H. Ye, Development of thermo-responsive polycaprolactone macrocarriers conjugated with Poly (N-isopropyl acrylamide) for cell culture, *Scientific reports* 9(1) (2019) 1-11.
- [67] S.L. Anna, N. Bontoux, H.A. Stone, Formation of dispersions using “flow focusing” in microchannels, *Applied physics letters* 82(3) (2003) 364-366.
- [68] S. van der Graaf, C. Schroën, R. Boom, Preparation of double emulsions by membrane emulsification—a review, *Journal of Membrane Science* 251(1-2) (2005) 7-15.
- [69] S.W. Choi, Y.C. Yeh, Y. Zhang, H.W. Sung, Y. Xia, Uniform beads with controllable pore sizes for biomedical applications, *Small* 6(14) (2010) 1492-1498.
- [70] S.W. Choi, I.W. Cheong, J.H. Kim, Y. Xia, Preparation of uniform microspheres

using a simple fluidic device and their crystallization into close-packed lattices, *Small* 5(4) (2009) 454-459.

[71] W.J. Seeto, Y. Tian, S. Pradhan, P. Kerscher, E.A. Lipke, Rapid Production of Cell-Laden Microspheres Using a Flexible Microfluidic Encapsulation Platform, *Small* 15(47) (2019) 1902058.

[72] B.G. Prajapati, M. Patel, A technology update: Electro spray technology, *International Journal of Pharmaceutical Sciences Review and Research* 1(1) (2010) 12-13.

[73] B.P. Pozniak, R.B. Cole, Perspective on electrospray ionization and its relation to electrochemistry, *Journal of the American Society for Mass Spectrometry* 26(3) (2015) 369-385.

[74] M. Yunmin, L. Yuanyuan, C. Haiping, H. Qingxi, Application and analysis of biological electrospray in tissue engineering, *The open biomedical engineering journal* 9 (2015) 133.

[75] Y.-S. Chen, Y.-S. Hsueh, Y.-Y. Chen, C.-Y. Lo, H.-C. Tai, F.-H. Lin, Evaluation of a laminin-alginate biomaterial, adipocytes, and adipocyte-derived stem cells interaction in animal autologous fat grafting model using 7-Tesla magnetic resonance imaging, *Journal of Materials Science: Materials in Medicine* 28(1) (2017) 18.

[76] B.A. Bunnell, M. Flaate, C. Gagliardi, B. Patel, C. Ripoll, Adipose-derived stem cells: isolation, expansion and differentiation, *Methods* 45(2) (2008) 115-120.

[77] S. Cheng, P.L. Wantuch, M.E. Kizer, D.R. Middleton, R. Wang, M. DiBello, M. Li, X. Wang, X. Li, V. Ramachandiran, Glycoconjugate synthesis using chemoselective ligation, *Organic & biomolecular chemistry* 17(10) (2019) 2646-2650.

[78] L. Wang, Y. Hou, X. Zhong, J. Hu, F. Shi, H. Mi, Preparation and catalytic



performance of alginate-based Schiff Base, Carbohydrate polymers 208 (2019) 42-49.

[79] R. Robitaille, J.F. Pariseau, F.A. Leblond, M. Lamoureux, Y. Lepage, J.P. Hallé, Studies on small (< 350 µm) alginate-poly-L-lysine microcapsules. III. Biocompatibility of smaller versus standard microcapsules, Journal of Biomedical Materials Research: An Official Journal of The Society for Biomaterials, The Japanese Society for Biomaterials, and The Australian Society for Biomaterials and the Korean Society for Biomaterials 44(1) (1999) 116-120.

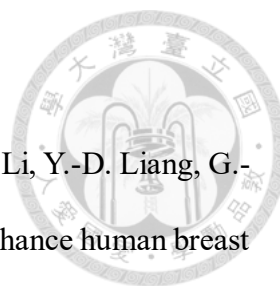
[80] E. Donnelly, M. Griffin, P. Butler, Breast Reconstruction with a Tissue Engineering and Regenerative Medicine Approach (Systematic Review), Annals of Biomedical Engineering (2019) 1-17.

[81] U. Rottensteiner, B. Sarker, D. Heusinger, D. Dafinova, S.N. Rath, J.P. Beier, U. Kneser, R.E. Horch, R. Detsch, A.R. Boccaccini, In vitro and in vivo biocompatibility of alginate dialdehyde/gelatin hydrogels with and without nanoscaled bioactive glass for bone tissue engineering applications, Materials 7(3) (2014) 1957-1974.

[82] F. He, C. Yu, T. Liu, H. Jia, Ginsenoside Rg1 as an Effective Regulator of Mesenchymal Stem Cells, Frontiers in pharmacology 10 (2020) 1565.

[83] W. He, W.-K. Wu, Y.-L. Wu, X.-H. Yang, Q.-X. Lin, W.-H. Yu, Ginsenoside-Rg1 mediates microenvironment-dependent endothelial differentiation of human mesenchymal stem cells in vitro, Journal of Asian natural products research 13(01) (2011) 1-11.

[84] N. Wang, C. Lu, X. Chen, Study on effect of ginsenoside Rg1 in promoting myocardial vascular endothelial cell regeneration through induction on bone marrow stem cell's migration and differentiation in rabbits of myocardial infarction, Zhongguo Zhong xi yi jie he za zhi Zhongguo Zhongxiyi jiehe zazhi= Chinese journal of integrated



traditional and Western medicine 25(10) (2005) 916-919.

[85] F.-T. Xu, Z.-J. Liang, H.-M. Li, Q.-L. Peng, M.-H. Huang, D.-Q. Li, Y.-D. Liang, G.-Y. Chi, D.-H. Li, B.-C. Yu, Ginsenoside Rg1 and platelet-rich fibrin enhance human breast adipose-derived stem cells function for soft tissue regeneration, *Oncotarget* 7(23) (2016) 35390.

[86] L.F. Yousif, J. Di Russo, L. Sorokin, Laminin isoforms in endothelial and perivascular basement membranes, *Cell adhesion & migration* 7(1) (2013) 101-110.

[87] T. Gloe, S. Riedmayr, H.-Y. Sohn, U. Pohl, The 67-kDa laminin-binding protein is involved in shear stress-dependent endothelial nitric-oxide synthase expression, *Journal of Biological Chemistry* 274(23) (1999) 15996-16002.

[88] Y.S. Chatzizisis, A.U. Coskun, M. Jonas, E.R. Edelman, C.L. Feldman, P.H. Stone, Role of endothelial shear stress in the natural history of coronary atherosclerosis and vascular remodeling: molecular, cellular, and vascular behavior, *Journal of the American College of Cardiology* 49(25) (2007) 2379-2393.

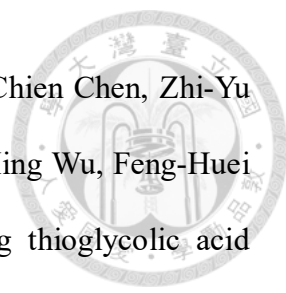
[89] S. Reakasame, A.R. Boccaccini, Oxidized alginate-based hydrogels for tissue engineering applications: a review, *Biomacromolecules* 19(1) (2017) 3-21.


## Publication list




### *i. Journal Papers*

1. **I-Hsuan Yang**, Makoto Sasaki, Kaho Takahashi, Koichiro Uto, Feng-Huei Lin, Mitsuhiro Ebara. “Fabrication of superabsorbent fibrous membranes via a homemade green centrifugal spinning system for the efficient removal of excess water in patients with kidney failure.” *Journal of Membrane Science*. 2023 October; 683:121871 [SCI, IF = 9.5, 4/86 (POLYMER SCIENCE, 4.1 %), Q1]
2. **I-Hsuan Yang**, Che-Yung Kuan, Zhi-Yu Chen, Chi-Han Li, Chih-Ying Chi, Yu-Ying Lin, Ya-Jyun Liang, Wei-Ting Kuo, Yi-An Li, Feng-Huei Lin. “Engineered cell-laden thermosensitive poly (N-isopropylacrylamide)-immobilized gelatin microspheres as 3D cell carriers for regenerative medicine.” *Materials Today Bio*. 2022 June; 15:100266 [SCI, IF = 8.2, 13/96 (ENGINEERING, BIOMEDICAL, 13.0 %), Q1, Times cited: 4]
3. **I-Hsuan Yang**, Yo-Shen Chen, Jia-Jing Li, Ya-Jyun Liang, Tzu-Chieh Lin, Subhaini Jakfar, Minal Thacker, Shinn-Chih Wu, Feng-Huei Lin. “The development of laminin-alginate microspheres encapsulated with Ginsenoside Rg1 and ADSCs for breast reconstruction after lumpectomy.” *Bioactive Materials*. 2021 June; 6(6):1699-1710 [SCI, IF = 18.9, 1/45 (MATERIALS SCIENCE, BIOMATERIALS, 1.1 %), Q1, Times cited: 16]
4. **I-Hsuan Yang**, I-En Lin, Tzu-Chien Chen, Zhi-Yu Chen, Che-Yung Kuan, Jhih-Ni Lin, Yu-Chia Chou, Feng-Huei Lin. “Synthesis, characterization, and evaluation of BDDE crosslinked chitosan-TGA hydrogel encapsulated with genistein for vaginal atrophy.” *Carbohydrate Polymers*. 2021 May 260:117832 [SCI, IF = 11.7, 3/86 (POLYMER SCIENCE, 2.9 %), Q1, Times cited: 10]

- 
5. **I-Hsuan Yang**, I-En Lin, Ya-Jyun Liang, Jhih-Ni Lin, Tzu-Chien Chen, Zhi-Yu Chen, Che-Yung Kuan, Chih-Ying Chi, Chi-Han Li, Hung-Ming Wu, Feng-Huei Lin. “Development of di(2-ethylhexyl) phthalate-containing thioglycolic acid immobilized chitosan mucoadhesive gel as an alternative hormone therapy for menopausal syndrome.” *Bioengineering & Translational Medicine*. 2021 November 7(2):e10267 [SCI, IF = 7.4, 18/96 (ENGINEERING, BIOMEDICAL, 18.2 %), Q1, Times cited: 3]
6. Tzu-Chieh Lin, Jhih-Ni Lin, **I-Hsuan Yang**, Christina Soong, Ya-Jyun Liang, Subhaini Jakfar, Chun-Che Yen, Hwa-Chang Liu, Hsuan-Yu Chen, Feng-Huei Lin. “The combination of resveratrol and Bletilla striata polysaccharide decreases inflammatory markers of early osteoarthritis knee and the preliminary results on LPS-induced OA rats.” *Bioengineering & Translational Medicine*. 2022 October e10431 [SCI, IF = 7.4, 18/96 (ENGINEERING, BIOMEDICAL, 18.2 %), Q1, Times cited: 2]
7. Subhaini Jakfar, Tzu-Chieh Lin, Zhi-Yu Chen, **I-Hsuan Yang**, Basri A Gani, Diana Setya Ningsih, Hendra Kusuma, Chia-Tien Chang, Feng-Huei Lin. “A Polysaccharide Isolated from the Herb Bletilla striata Combined with Methylcellulose to Form a Hydrogel via Self-Assembly as a Wound Dressing” *International Journal of Molecular Science*. 2022 October 23(19):12019 [SCI, IF = 5.6, 66/285 (BIOCHEMISTRY & MOLECULAR BIOLOGY, 23.0 %), Q1, Times cited: 3]
8. Tzu-Chien Chen, Rui-Chian Tang, Jhih-Ni Lin, Wei-Ting Kuo, **I-Hsuan Yang**, Ya-Jyun Liang, Feng-Huei Lin. “The synthesis and evaluation of thiolated alginate as the barrier to block nutrient absorption on small intestine for body-weight

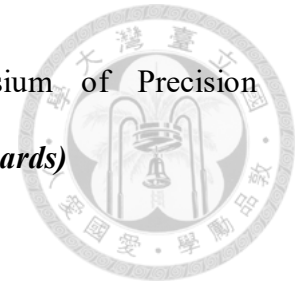
- 
- control.” *Bioengineering & Translational Medicine*. 2022 August, e10382 [SCI, IF = 7.4, 18/96 (ENGINEERING, BIOMEDICAL, 18.2 %, Q1)]
9. Chi-Han Li, **I-Hsuan Yang**, Cherng-Jyh Ke, Chih-Ying Chi, Jefunnie Matahum, Che-Yung Kuan, Nehar Celikkin, Wojciech Swieszkowski, Feng-Huei Lin. “The production of fat-containing cultured meat by stacking aligned muscle layers and adipose layers formed from gelatin-soymilk scaffold.” *Frontiers in Bioengineering and Biotechnology*. 2022 April 10:875069 [SCI, IF =5.7, 16/73 (MULTIDISCIPLINARY SCIENCES, 21.2 %), Q1, Times cited: 6]
10. Ya-Jyun Liang, Jia-Yu Hong, **I-Hsuan Yang**, Xin-Ran Zhou, Yi-Wen Lin, Tzu-Chieh Lin, Chun-Han Hou, Feng-Huei Lin. “To Synthesize Hydroxyapatite by Modified Low Temperature Method Loaded with Bletilla striata Polysaccharide as Antioxidant for the Prevention of Sarcopenia by Intramuscular Administration.” *Antioxidants*. 2021 March 10(3):488 [SCI, IF = 7.0, 13/142 (FOOD SCIENCE & TECHNOLOGY, 8.8 %), Q1, Times cited: 10]
11. Ya-Jyun Liang, **I-Hsuan Yang**, Yi-Wen Lin, Jhih-Ni Lin, Chang-Chin Wu, Chih-Yung Chiang, Kun-Hung Lai, Feng-Huei Lin. “Curcumin-Loaded Hydrophobic Surface-Modified Hydroxyapatite as an Antioxidant for Sarcopenia Prevention.” *Antioxidants*. 2021 April 10(4):616 [SCI, IF = 7.0, 13/142 (FOOD SCIENCE & TECHNOLOGY, 8.8 %), Q1, Times cited: 7]
12. Tzu-Chien Chen, Yu-Yu Ho, Rui-Chian Tang, Yong-Chen Ke, Jhih-Ni Lin, **I-Hsuan Yang**, Feng-Huei Lin. “Thiolated Chitosan as an Intestinal Absorption Carrier with Hesperidin Encapsulation for Obesity Treatment.” *Nutrients*. 2021 December 13(12):4405 [SCI, IF =5.7199, 17/88 (NUTRITION & DIETETICS, 18.7 %), Q1, Times cited: 3]

- 
13. Che-Yung Kuan, Yu-Ying Lin, **I-Hsuan Yang**, Ching-Yun Chen, Chih-Ying Chi, Chi-Han Li, Zhi-Yu Chen, Li-Ze Lin, Chun-Chen Yang, Feng-Huei Lin. “The Synthesis of Europium-Doped Calcium Carbonate by an Eco-Method as Free Radical Generator Under Low-Intensity Ultrasonic Irradiation for Body Sculpture.” *Frontiers in Bioengineering and Biotechnology*. 2021 November 9:765630 [SCI, IF=5.7, 16/73 (MULTIDISCIPLINARY SCIENCES, 21.2 %), Q1]

*ii. Conference Papers*

1. **I-Hsuan Yang**, Makoto Sasaki, Mitsuhiro Ebara. “Design strategy for Nanostructured Porous Carbon Nanofibers from Bio-Resource Chitosan Loaded with Nitrogen-Doped Zeolites as Effective Adsorbents for Chronic Kidney Failure Patients” 2023 72nd The Society of Polymer Science Annual Meeting, Japan (2023 SPSJ). (Oral presentation)
2. **I-Hsuan Yang**, Makoto Sasaki, Mitsuhiro Ebara. “Design of functionalized poly(acrylic acid)-ethylene glycol fiber meshes via centrifugal spinning to remove excess water from kidney failure patients” Tsukuba Biomedical Engineering Forum 2023, Japan (Poster)
3. **I-Hsuan Yang**, Min-Hua Chen, Feng-Huei Lin. “Development of ROS-generated nanoparticles with gamma radiation for lung cancer therapy” 2021 The 6th International Symposium on Radiation Education, Taiwan (2021 ISRE). (***Best Poster Award***)
4. Chia-Tien Chang, Che-Yung Kuan, Ching-Yun Chen, Zhi- Yu Chen, **I-Hsuan Yang**, Chih-Chieh Chen, Chih-Wei Lin, Yue-Leon Guo, Chi-Hsien Chen, Feng-Huei Lin. “Development of a new filter materials with effective VOCs adsorption

and particulate filtration” 2021 International Symposium of Precision Environmental Medicine, Taiwan (2021 ISPEM). (*Poster Awards*)



*iii. Awards*

1. Poster Awards, “Development of a new filter materials with effective VOCs adsorption and particulate filtration” 2021 International Symposium of Precision Environmental Medicine, Taiwan.
2. Best Poster Award, “Development of ROS-Generated Nanoparticles with Gamma Radiation for Lung Cancer Therapy” The 6th International Symposium on Radiation Education, Taiwan, 2021.
3. Awarded for International Cooperative Graduate Program (ICGP) Fellowship under the “National Taiwan University - NIMS Cooperative Graduate Program, Japan, 2022.
4. Awarded for Lin’s Scholarship National Taiwan University Project as an overseas visiting student, 2019